NASA CR-132719

DEVELOPMENT OF A STRATOSPHERIC AND MESOSPHERIC MICROWAVE TEMPERATURE SOUNDER EXPERIMENT

By D. H. Staelin, P. W. Rosenkranz, B. G. Anderson, K. F. Kunzi, R. M. Paroskie, R. J. Parr, and J. W. Waters

Prepared under Contract No. NAS1-10693 by

Research Laboratory of Electronics
Massachusetts Institute of Technology
Cambridge, Massachusetts 02139

for

NATIONAL AERONAUTICS AND SPACE ADMINISTRATION

FINAL REPORT

National Aeronautics and Space Administration

Contract NAS1-10693

covering the period

June 25, 1971 - June 30, 1975

TABLE OF CONTENTS

ABSTRACT

A passive microwave spectrometer system for measuring global atmospheric temperature profiles 0-75 km altitude was developed and analyzed. The system utilizes 12 channels near the 5-mm wavelength oxygen absorption band and is designed to provide global coverage by scanning perpendicular to the orbital track of a polar orbiting satellite. The experiment could be used for scientific or operational purposes.

A significant improvement in the accuracy of theoretical atmospheric microwave transmittance functions was achieved through development of a new first-order approximation to overlapping line theory for the O_2 molecule. This approximation is particularly important in the troposphere and lower stratosphere where pressure-broadening blends nearby lines. This new precision in microwave transmittances is an advantage relative to the present uncertainties in infrared temperature sounding systems. Ground-based and aircraft observations of several resonances of stratospheric oxygen generally support the new theory. The 23_, 25_, 29_, and 31_ atmospheric oxygen lines were measured for the first time and the frequencies of several such oxygen lines were measured with improved precision. The polarization and Zeeman splitting of the atmospheric 27_ line was also observed for the first time.

I. Introduction

The Massachusetts Institute of Technology and the California Institute of Technology Jet Propulsion Laboratory undertook a four year program to develop a space experiment that would employ a 5 mm wavelength spectrometer to infer the temperature profile in the stratosphere and mesosphere.

The program included 1) improvements and extension of pressure broadening theory to predict the microwave spectrum of oxygen in the atmosphere; 2) development of techniques for interpreting the microwave spectral data in terms of atmospheric temperature profiles; 3) construction of a flexible 23-channel microwave spectrometer; 4) ground- and aircraft- based measurements using this spectrometer to test the theories; 5) design of a space experiment; and 6) construction at J. P. L. of breadboard and engineering models of a simpler instrument designed for spaceflight (but not spacequalified). The operating frequencies of the J. P. L. instruments will be shifted to permit sounding of atmospheric temperatures up to 50 km from the ground. This report summarizes the results of those aspects (1-5) of the work that were carried out at M. I. T.

The principal achievements of the experimental program were these: the 29_ and 31_ oxygen lines were measured for the first time. The 23_ and 25_ lines were measured for the first time in the atmosphere. Frequencies of the 25_ and 27_ lines were determined with greater accuracy than previously obtained. The first measurements of polarization and Zeeman splitting of the 27_ line in the atmosphere were made. The possibility of inferring temperature variations at 40 to 50

km altitudes from microwave measurements was demonstrated.

The theoretical work produced a simplified formulation of overlapping line theory that is useful in calculation of microwave absorption in the atmosphere. Interference effects that arise when the oxygen lines overlap (in the troposphere) are included. For ground-based measurements the isolated line emission from the upper stratosphere is attenuated by the troposphere, and in a space experiment the troposphere would be seen as a background. Using the results of laboratory spectroscopic measurements by H. J. Liebe at the Institute for Telecommunications Sciences, Boulder, Colorado, in these theoretical expressions gives improved agreement with our measurements, in comparison with older theoretical calculations.

Publications by Waters (1973) and Rosenkranz (1975) described research done under this contract.

II. Measurements of Atmospheric Oxygen Lines

A. Radiometer System

The receiver constructed for measurements of upper stratospheric temperature consists of a Dicke-switched microwave radiometer covering the frequency range of approximately 50-55 GHz, a filter bank for spectral analysis at the 60 MHz i.f. frequency, and a small computer and magnetic tape recording system for processing and recording data. The radiometer is unique in that its mixer-preamp represent state-of-the-art microwave receiver technology. The mixer was constructed at M. I. T. Lincoln Laboratory by R. W. Chick and the preamplifier was constructed in our group at R. L. E. by V. T. Kjartansson. In addition to processing and storing data, the small computer controls automatic calibration of the radiometer during observations and produces a real-time display of the observed spectra.

A block diagram of the radiometer is given in figure 2.1 and a photograph in figure 2.2. During observations the radiometer is mounted in a tiltable, insulated box. The filter bank block diagram is shown in figure 2.3. The overall noise temperature of the receiver at 53 GHz was $\sim$1900^{o}K as determined from calibrated noise measurements.

The absolute calibration of the receiver was accomplished by looking at known input temperatures of +100^{o}C (hot load), 25^{o}C (ambient), and 77^{o}K (liquid nitrogen), and computing values for the internal calibration signal. From the observed difference

between hot load and ambient a value of 128°K was inferred for the internal calibration. From the observed difference between liquid nitrogen and ambient a value of 106°K was inferred for the internal calibration. (The same value was obtained by observing the liquid nitrogen temperature with horn antenna looking at absorber apikes inside a dewer filled with liquid nitrogen, and by looking at a waveguide termination cooled externally with liquid nitrogen.) The spectra shown in subsection II-B of this report were obtained using a value of 115°K for the internal calibration and hence may have an absolute error of ± ∿10 %. The calibration problem is discussed further in subsection II-D.

The minicomputer data processing system is shown in figure 2.4. From top to bottom, the components are: a dual drive Linc magnetic tape system, filter bank, Data General Nova 1200 minicomputer with 8K of memory, and a Compu Systems 10 bit analogue to digital converter with 32 channel multiplexer. Not shown is an ASR 33 teletype. Internal to the system is a real-time clock which interrupts the software each 0.10 seconds and a homemade computer interface which allows the computer (1) to send out or read in a Dicke switch reference and (2) to send out mechanical switch control signals, thereby controlling the calibration state of the radiometer.

A flowchart of the basic software for acquisition, processing, storage, and display of receiver data is given in figure 2.5. Since the processor generates the mechanical switch position and ferrite switch position, it knows whether the data is calibration data or

antenna data and whether the Dicke switch is in the signal mode or the comparison mode. The remainder of the software's job is to keep track of the various kinds of data, integrate data for a predetermined integration time, and average the integrated data. During half of a Dicke cycle, each of the 24 data channels is read 8 times; this takes approximately 5 milliseconds which results in a Dicke switch frequency of approximately 100 hertz. Each 30 seconds, the contents of the monotonically increasing "SUM" registers is recorded on magnetic tape for future reference. When averages of all calibration data are available, gains and system temperatures are calculated for each of the 24 channels and are stored in memory and on magnetic tape. When averages of antenna data are available, signal minus comparison is calculated, stored on magnetic tape and plotted out on the teletype. After plotting the results, the processor observes the switches on the minicomputer console. A predetermined combination of the switches will terminate the experiment; otherwise, the next calibration sequence is started.

Extended software is available which provides programmed "HALT"'s in the situation where the mechanical switch must be manually changed and which provides the capability to observe instead of generate the Dicke reference in the situation where the reference must be generated external to the computer.

B. Ground-based Measurements (1972)

The receiver system described in the previous subsection was used to observe atmospheric emission from five of the oxygen lines

(fig. 2.6). The frequency of the 27 line was measured much more accurately than when the line was first detected (Waters, 1970). Atmospheric emission from the 23_, 25_, 29_, and 31_ O_2 lines was measured for the first time. These observations are described in detail by Waters (1973). The calculations shown in this subsection used the linewidth given by Reber (1972), rather than the more recent formulation described in section III. The discrepancy between measurement and calculation is discussed in subsection II-D.

The radiometer system was taken to Arecibo Observatory (Puerto Rico) in October, 1972, and measurements were made of atmospheric emission from the five high-J O_2 lines. The purpose of the measurements from Arecibo was to observe the predicted narrowing of the lines (because of less separation of the Zeeman components) in the weaker magnetic field at Arecibo, and to look for the slight linear polarization in the emission from the lines expected at low magnetic latitudes.

Figure 2.7 shows measurements of the 27_ line made at Arecibo with the filter system. For comparison, the line measured at Haystack is also shown. The Arecibo line is narrower than the Haystack line by approximately the expected amount, although both lines are stronger than calculated. The difference in the two linear polarizations observed at Arecibo is also given in fig. 2.7 and is larger than calculated by approximately the same amount as the amplitudes. The two linear polarizations were observed by rotating the radiometer so that the linearly polarized horn antenna

produced a measured electric field which was alternately parallel and perpendicular to the terrestrial magnetic field. The direction of the magnetic field was taken to be that at the surface measured by a simple hand compass. The switching period between the two polarizations was 10 min. The calculated polarization difference shown in fig. 2.7 assumed a magnetic latitude of 29° and a 15°N annual average temperature model, corresponding to conditions at Arecibo. Higher resolution measurements were also made of the 27_ line with the Arecibo autocorrelator, and the results are compared with the Haystack autocorrelator measurements in fig. 2.8. The correlator measurements at Arecibo were made with the assistance of Dr. Alan Parrish of the Arecibo Observatory staff.

A significant result of these measurements is accurate center frequencies for the 23_ to 31_ lines. The measured frequencies, listed in table II-1, are in good agreement with calculations by Wilheit (1970) and Welch and Mizushima (1972). A 3.5 MHz error in Mizushima and Hill's (1954) measurement of the 25_ line was found.

C. Aircraft-based Measurements

These observations were made during the joint Soviet-American Bering Sea Expedition (BESEX) of February - March 1973. The test platform was NASA 711, a Convair 990 specially equipped for atmospheric and surface research. Microwave emission from the 25_ line was measured using the radiometer system with an antenna looking upward at 65° elevation through a port in the fuselage.

Table II-1. Oxygen line frequencies.

line	frequencies (MHz)			
	measured		calculated	
	Waters (1973)	Mizushima & Hill (1954)	Wilheit (1970)	Welch & Mizushima (1972)
23_	54130.2 ± .5	54129.4 ± .4	54129.956	54129.962
25_	53595.9 ± .2	53599.4 ± .8	53595.678	53595.682
27_	53066.9 ± .2		53066.799	53066.802
29_	52542.4 ± .2		52542.237	
31_	52021.4 ± .5		52021.192	

Missions were flown as shown in fig. 2.9, over the southwestern U. S., along a track from San Francisco to Anchorage, over Alaska and the Bering Sea, over polar ice in the Arctic, and along a track from Anchorage to Hawaii. The observations have been described in detail by Anderson (1973) and in the second Interim Yearly Report for this contract. The objectives were: (1) to study line shape and strength including Zeeman effects, (2) to observe stratospheric temperature variations in space and time, and (3) to study tropospheric opacity under different climatic conditions.

To derive the actual brightness temperature spectra (with arbitrary baselines) from the radiometric measurements it is necessary to multiply the measurement spectra by several factors. The first of these is a factor of 2 because the spectral feature exists in only one sideband of the radiometer. The second is a factor for the waveguide loss. In the case of BESEX flight 1 (with an extra isolator in the antenna line), this factor is 2. For the other flights this factor is 1.6, corresponding to a 2 dB loss in the waveguide. The last factor is a correction for the radiometer calibration. There is considerable uncertainty in the value of this factor. Ground-based calibration studies indicate 0.95 $\pm$5 % as a reasonable value. BESEX flight 1 data indicate a value of 0.715 $\pm$15 % while BESEX flight 13 indicates a value of 0.91 $\pm$10 %. Considering all of these, a factor of 0.8 $\pm$15 % was used.

Figure 2.10 shows the variation in line brightness with

altitude, due to attenuation in the lower atmosphere. Again, all of the calculated spectra in this subsection were computed with the old oxygen absorption coefficient expressions. The tropospheric opacity inferred from the data in fig. 2.10 is in agreement, within measurement uncertainty, with expected values.

Figure 2.11 illustrates the narrowing and intensification of the line with decreasing latitude. This is caused by the decrease in magnetic field strength and changing atmospheric temperature profile.

Stratospheric temperatures inferred from the line measurements are presented in fig. 2.12 as a function of latitude and in fig. 2.13 as a function of time. Interpretation of line profiles by means of contribution functions, weighting the atmospheric temperature profile, has been discussed by Waters (1970) and in the First Interim Yearly Report for this contract. Briefly, if the line brightness 2.5 MHz from center is subtracted from the brightness at line center, the difference is most sensitive to atmospheric temperature at an altitude of 50 km, with a spread of $\pm$8 km. The difference between brightness at 2.5 MHz and 20 MHz from line center is most sensitive to atmospheric temperature at 40 km, with spread of $\pm$9 km. A change of 1 % in atmospheric temperature produces a 4 % change in brightness of the 25_ line, due to the Maxwellian population distribution among the rotational states of oxygen. For comparison figures 2.12 and 2.13 also show measurements with rocketsondes and by the Selective Chopper Radiometer (SCR) on Nimbus-5. Although

the data is somewhat noisy, the trend of inferred temperature agrees well with the comparison measurements. These figures demonstrate the potential of oxygen line measurements as indirect probes of upper stratospheric temperature variations.

D. Recent Ground-based Measurements (1975)

In September 1974, new diodes from Lincoln Laboratory were installed in the mixer. An initial observation of the 25_ line proved successful. The plan at this point was to obtain data on the calibration accuracy of the instrument and to make a series of observations, to check the previous observations (section II-B). However, a larger than expected drift component in the radiometer data was encountered. The drift affected both the radiometer channel gains and the instrument baseline. Subsequent to the observations reported here, this problem was solved by relocating the ferrite switch driver to the computer rack. Additional observations are planned.

The method of taking data was designed to minimize the adverse effects of drift. A single instrument calibration using warm and ambient absorbing loads at the antenna was run at the start of the observation procedure. After that, a number of cycles of relatively short observations were made. Each cycle consisted of an atmospheric line observation, a warm and an ambient load observation, and an ambient load observation with the noise tube switched on. The respective mean was subtracted from each set of data, and the result was averaged over each

channel (obtaining also the standard deviation). The mean over all observations was then added to the channel means for each type of data. The hot and ambient load data averaged over each channel was used to obtain a correction for the gain calibration. The final result for each channel was computed from

$$T_A = (T_L - T_{AMB}) \left(\frac{T'_{HOT} - T'_{AMB}}{T_{HOT} - T_{AMB}}\right) \qquad (2.1)$$

where

T_L = averaged line data

T_{AMB} = averaged ambient load data

T_{HOT} = averaged hot load data

T'_{HOT} = measured (via a digital thermometer) hot load temperature

T'_{AMB} = measured ambient load temperature

Figure 2.14 shows the April 1975 observations. The data taken on April 28 and 29 had large baseline tilts; this tilt was assumed to originate in the equipment and was subtracted before averaging. These measurements confirm the 1972 measurements, shown for comparison. The DC level of all of the plots in fig. 2.14 is arbitrary and has been adjusted to place channel # 1 at zero. This should be borne in mind when interpreting the observational data, since the standard deviation of this channel may adjust the apparent line height. In addition, inaccuracies may be present in the observational data due to the drift problem

discussed above; standard deviations for the channel averages range from approximately 0.5^{o} to 2.0^{o} K. Nevertheless, the line data presents apparently far less ripple than this. Perhaps varying baseline characteristics, which are not removed from the data until after the standard deviations have been taken, account in part for the high and irregular standard deviations.

At approximately the time the experimental program was restarted, an improved formulation of the oxygen absorption coefficient was developed (Rosenkranz, 1975). This formulation treats the effect of overlapping lines to first order in pressure. Also, high-precision measurements of oxygen linewidths by Liebe (1975) indicated a gradual decrease in linewidth with increasing rotational quantum number, whereas our previous computations had assumed the same collisional linewidth parameter for all lines. At present, Liebe has measured lines with quantum numbers N = 3 to 9 and finds a linear decrease with N. Extrapolation of this trend to the 25_ line implies a width 16 % less than we had previously assumed.

The "new theory" calculation in fig. 2.14 uses overlapping line theory with Liebe's linewidths, as described in Section III; the "old theory" uses the Meeks and Lilley (1963) model. The new calculation removes about half of the previous discrepancy between theory and measurement. This change evidently is due to the narrower linewidth parameter, since tropospheric opacities computed from the two models happen to be virtually the same at this frequency. Because of the way the line forms in the atmosphere,

the narrower linewidth parameter has the effect of making the line appear stronger within our 40 MHz window. (The line shape near the center, as seen in fig. 2.8, is determined by Zeeman splitting rather than collision broadening.)

We see that the linewidth parameter is a source of uncertainty in the calculations. This line is so weak that it would be very difficult to measure in the laboratory. We could interpret our atmospheric measurements as implying an even narrower linewidth parameter than currently assumed. However, we have no way of determining the temperature dependence, which the calculations still assume to be the same as for the stronger lines. Theoretical calculations of line widths (e.g., Mingelgrin, 1972; Dillon and Godfrey, 1972; Barrett and Lam, 1975) could help to resolve this problem, but there is disagreement among these also. Fortunately, a space experiment, as described in section IV, would make use of the stronger lines, which have been measured in the laboratory.

III. OXYGEN ABSORPTION COEFFICIENT

A. Tropospheric Opacity

At pressures on the order of an atmosphere, the oxygen spin-multiplet spectrum merges into a band centered at 60 GHz. At any given frequency, absorption is contributed by several lines. Under these conditions, molecular collisions that change the rotational quantum number of the radiating oxygen molecule do not broaden the spectrum as much as they do for resolved lines.

Pressure-broadening may be described as a Markov random process of intensity transfer among the lines (see Gordon, 1966, and references therein). The absorption coefficient is given by

$$\gamma = CP\left(\frac{\nu}{T}\right)^2 \mathrm{Im}\mathrm{Tr}[\underline{\underline{\Phi}}\underline{d}\underline{d}^t(\nu\underline{\underline{I}} - \underline{\underline{\nu}} - iP\underline{\underline{W}})^{-1}] \qquad (3.1)$$

where C is a constant, ν is frequency, P is pressure, T is temperature, $\underline{d}$ is a column vector of line amplitudes, $\underline{\underline{\nu}}$ is a diagonal matrix of line frequencies, $\underline{\underline{\Phi}}$ is a diagonal matrix whose elements are the fractional populations of the initial states of the lines, and $\underline{\underline{I}}$ is the identity matrix. The product $2\pi P\underline{\underline{W}}$ is a transition rate matrix for the Markov process: an off-diagonal element gives the negative of the rate of intensity transfer from the line associated with its column to the line associated with its row; a diagonal element gives the total rate of transfer of intensity from its associated line to all other lines. Thus the diagonal elements of $\underline{\underline{W}}$ are line halfwidths per unit pressure for the resolved spectrum.

By using first-order perturbation theory, eq. 3.1 can be approximated by (Rosenkranz, 1975):

$$\gamma = C\left(\frac{\nu P}{T}\right)^2 \sum_k \Phi_k \frac{w_{kk} d_k^2 + (\nu - \nu_k)\, y_k}{(\nu - \nu_k)^2 + (P w_{kk})^2} \qquad (3.2)$$

where the coefficients of the interference terms are given by

$$y_k = 2\, d_k \sum_{j \neq k} \frac{d_j w_{jk}}{\nu_k - \nu_j} \qquad (3.3)$$

We now introduce a slightly different notation for ease of enumeration of the oxygen lines. Let N be the rotational quantum number (only odd values are allowed). An absorption transition in which the spin is reoriented with respect to rotational angular momentum, changing the total angular momentum from J = N - 1 to J = N, is denoted by ν_N^-. Likewise, for J = N + 1 → J = N we have ν_N^+. Since the absorption coefficient is proportional to ν^2 times the fourier transform of the dipole moment autocorrelation function, it must be an even function of ν. This symmetry is provided by (emission) lines at $-\nu_N^-$ and $-\nu_N^+$. There also is nonresonant absorption, represented by two "lines" at zero frequency for each rotational state. Since these latter lines are never resolved, transfer of intensity among them (i.e., by changes in rotational state) has no broadening effect. Consequently the nonresonant halfwidth is

$$w_b = \sum_j w_{jk} \quad \text{for } \nu_j = 0,\ \nu_k = 0 \qquad (3.4)$$

Most of the oxygen lines cluster around 60 GHz, the one exception being the 1^- line at 118.75 GHz. We note from eq. 3.3 that the contribution from negative frequency lines to interference coefficients for positive frequency lines can therefore be computed to a good approximation by summing the corresponding elements of $\underline{W}$ and using an average frequency. (The d's are all close to unity.) Gordon's (1967) theory predicts

$$\sum_j W_{jk} = -\frac{1}{2} W_b \quad \text{for } \nu_j < 0,\ \nu_k > 0 \tag{3.5}$$

Similarly, for the zero frequency lines:

$$\sum_j W_{jk} = -\frac{1}{2} W_b \quad \text{for } \nu_j = 0,\ \nu_k \neq 0 \tag{3.6}$$

Next we consider interference among the lines at positive frequencies. Analogously to eq. 3.4, Gordon's theory predicts

$$\sum_j W_{jk} = W_b \quad \text{for } \nu_j > 0,\ \nu_k > 0 \tag{3.7}$$

Since W_b describes the effective halfwidth of the resonant band as a whole (in the wings) as well as the nonresonant component, it might be called a "bandwidth parameter". Computations by Barrett and Lam (1975) indicate that diagonal and near-diagonal elements are dominant in the $\underline{W}$ matrix for oxygen. In other words, the lines are weakly coupled. We therefore set to zero all remaining elements in $\underline{W}$, as in fig. 3.1. The near-diagonal elements defined in fig. 3.1 can be determined from the diagonal elements W_b and W_N by the following recursive equations:

$$w_{39}^{\uparrow} = 0 \qquad (3.8)$$

$$w_N^{\downarrow} = w_b - w_N - w_N^{\uparrow} \qquad (3.9)$$

$$w_{N-2}^{\uparrow} = w_N^{\downarrow} \frac{\Phi_N}{\Phi_{N-2}} \qquad (3.10)$$

Eq. 3.9 follows from eq. 3.7, and eq. 3.10 follows from the requirement that the product $\underline{W}\,\underline{\Phi}$ be symmetric in order to maintain detailed balance. Eq. 3.8 is introduced arbitrarily but is noncritical. These approximations are discussed at greater length by Rosenkranz (1975).

The motivation for all of the above approximations is that they permit computation of the oxygen absorption coefficient from laboratory measurements of linewidths. Liebe (1975) gives the following empirical equation for the oxygen halfwidths in air:

$$w_N = (1.38 - 0.016\ N)\ (300/T)^{0.85}\ \text{(MHz/mb)} \qquad (3.11)$$

This equation is based on measurements of lines with N = 3 to 9 and its extrapolation is one of the major sources of uncertainty in interpretation of the measurements of high N lines described in the previous section. For the nonresonant halfwidth we average measurements by Kaufman (1967) and Maryott and Birnbaum (1960):

$$w_b = 0.48(300/T)^{0.89}\ \text{(MHz/mb)} \qquad (3.12)$$

Now, to write eq. 3.3 explicitly, the interference coefficients for positive frequency lines are:

$$y_N^{\pm} = d_N^{\pm}\left\{\frac{2d_{N+2}^{\pm}\ w_N^{\uparrow}}{\nu_N^{\pm} - \nu_{N+2}^{\pm}} + \frac{2d_{N-2}^{\pm}\ w_N^{\downarrow}}{\nu_N^{\pm} - \nu_{N-2}^{\pm}} - \frac{w_b}{\nu_N^{\pm}} - \frac{w_b}{\nu_N^{\pm} + 60}\right\} \qquad (3.13)$$

where -60 GHz is used as an average frequency for all negative frequency lines. The coefficients for negative frequency lines are equal to -1 times the coefficients for corresponding positive lines and the coefficient for the nonresonant term cancels, because of symmetry.

On the wings of the oxygen band the sum of all the antisymmetric terms in eq. 3.2 leaves a residual that subtracts from the resonant (Lorentzian) contribution. The band as a whole behaves as though it has the same width parameter as the nonresonant component, i.e. according to eq. 3.7.

Now we wish to consider how opacities computed from eqs. 3.2 and 3.13 differ from results obtained with earlier models such as those of Meeks and Lilley(1963) and Reber (1972). The latter two models account for the low absorption on the wings of the band by making the individual linewidths nonlinear functions of pressure. Over the range 50 to 54 GHz tropospheric opacities differ by no more than 5 % among the three models. On the other hand, when the lines are partially resolved, as in fig. 3.2, a difference is seen in the two approaches at 58.8 GHz. Compared with a sum of Lorentzian lineshapes, eqs. 3.2 and 3.13 predict more absorption and the other two models less at this frequency, which lies in the valley between the 3^+ and 7^- lines. The agreement with mea-

surements demonstrates that the low absorption on the wings of the band is due to transfer of intensity from the wings to the center, rather than a decrease in individual linewidths.

B. Stratospheric and Mesospheric Opacity

At altitudes above ∿25 km the lines are narrow and appreciable absorption occurs only near line centers. In eq. 3.2 the interference terms contain the factor $(\nu - \nu_k)$ so near the center the line shapes are nearly Lorentzian.

At altitudes above ∿40 km Zeeman splitting of the lines, caused by the earth's magnetic field, contributes substantially to their observed width (and shape). Components of emission lines for which the change in M (quantum number for the projection of molecular magnetic moment along the external magnetic field) is zero are linearly polarized with the E vector perpendicular to the external magnetic field. Components for which $\Delta M = \pm 1$ are in general partially polarized. To treat this problem it is necessary to use the tensor formulation of radiative transfer, in which absorption is described by a coherency matrix (Lenoir, 1967, 1968).

Lenoir's formulation addresses the problem of coherency between polarizations but assumes no coherency between different Zeeman components; i.e., a sum of Lorentzian shapes is used. A completely general formulation within the framework of overlapping line theory would apparently require replacement of eq. 3.1 with

a matrix equation in which each element of $\underline{W}$ becomes a sixth-rank tensor, describing the coupling between all combinations of Zeeman components and polarizations.

However, if we consider a definite polarization, it must be possible to think of the process of merging of Zeeman components within each line as analogous to the merging of lines within the band. In the latter case, coherency between the lines has the effect of making the band effectively narrower than its components. The effect is a factor of $\sim$2 and is quite significant for atmospheric radiation computations. We can estimate the size of such an effect for the Zeeman components by comparing Liebe's (1975) zero-field linewidth measurements with measurements of collisional electron paramagnetic resonance linewidths by Gardiner et al. (1975). (In an accompanying paper, Pickett (1975) discusses the relation between millimeter wave and EPR linewidths). The latter show a marginally significant ($\sim$5 %) dependence on M, and the average linewidths for N = 7 and 9 are $\sim$5 % higher than Liebe's measurements. Both experimenters claim uncertainties of typically $\sim$2 %. We infer from these measurements an upper limit of $\sim$10 % on a possible coherency between the Zeeman components. This would probably be too slight to appreciably affect the results of our atmospheric radiation computations. Therefore we shall continue to use Lenoir's formulation in the Zeeman-splitting region of the atmosphere.

At altitudes above $\sim$70 km Doppler broadening of the Zeeman

components becomes appreciable compared to collision broadening. The Doppler effect can be computed from first principles. The resulting Voigt lineshape is a convolution of the Doppler (gaussian) and collisional lineshapes (Lenoir, 1968). To economize on computer time we make the approximation of combining Doppler and collision linewidths in quadrature and use the Lorentz lineshape.

IV. Proposed Space Experiment

A. Weighting functions

Table IV-1 lists channel frequencies and bandwidths for a space-based temperature sounder, Channels 8-12 would be single conversion channels and would each have two sidebands. Channels 1-7 would be dual conversion, with four sidebands each. The antennas would scan in 13 steps of 7.2^{o}, giving extreme positions of 43.2^{o} to left and right of nadir (similar to the Nimbus F microwave spectrometer). This experiment would measure the 7^{-} and 5^{+} lines with channels 1-9, as shown in fig. 4.1. The figure shows the total intensity of brightness temperature, but one should keep in mind that the radiation is partially polarized near the line centers. The choice of these two lines is motivated by the fact that, except for the doublets (which are too close together), they are the closest pair of strong oxygen lines and provide the only "valley" for which the channel 9 weighting function will peak above 20 km at nadir. With 12 channels, this gives a reasonably uniform spacing of the weighting functions.

An alternate version of the experiment could use two of the weaker lines (e.g. 11^{-} and 13^{-}) thus moving channels 1-9 downward, and eliminating channel 12. This version would eliminate the power requirement for one local oscillator, but would sacrifice 5 km of the maximum height sounded.

Shown in figs. 4.2(a) and 4.2(b) are nadir weighting functions at the magnetic equator for linear polarization with the E-vector respectively parallel and perpendicular to the earth's magnetic

Table IV-1. Experiment specifications. Noise is calculated on the assumption of a 1400 K radiometer noise temperature and 250 K antenna temperature. Channel 9 is assumed to be 10 percent worse and channels 1-8 20 percent worse due to higher i. f. preamplifier noise figures. The integration time is that for the Tiros- N microwave spectrometer.

Channel No.	Passband center frequencies (MHz)	IF bandwidth (MHz)	RMS noise for 1.84 sec integration (K)
1	59377.60 ± 213.38 ± 0.42	0.64	2.76
2	59377.60 ± 213.38 ± 1.2	1.0	2.21
3	59377.60 ± 213.38 ± 2.1	1.0	2.21
4	59377.60 ± 213.38 ± 3.75	2.0	1.56
5	59377.60 ± 213.38 ± 6.1	2.5	1.40
6	59377.60 ± 213.38 ± 8.7	3.6	1.16
7	59377.60 ± 213.38 ± 17.0	10.0	0.69
8	59377.60 ± 176	30	0.57
9	59377.60 ± 60	100	0.29
10	52850 ± 60	100	0.26
11	53850 ± 60	100	0.26
12	55450 ± 60	100	0.26

field. These weighting functions are averaged over the channel bandpasses. It may be seen that there is a slight difference in channels 1-3. For this particular case (direction of propagation perpendicular to the magnetic field) there is no circular component of brightness temperature. In general, the circular component is antisymmetric about the line centers; i.e. it reverses sense from left to right as one scans the line. Since our bandpasses are symmetric about the line centers, we cannot detect the circular component with any choice of antenna polarization. The linear components are symmetric about the line centers, though, so a linearly polarized antenna would see a brightness temperature that depends on its orientation with respect to the earth's field. The latter would depend on the spacecraft orbit. These considerations lead us to the choice of a circularly polarized antenna (either left or right). This choice results in a slight degradation of vertical resolution near the equator due to averaging of the two linear components, but greatly simplifies data interpretation. Over the magnetic poles the choice of polarization makes no difference, since the linear component disappears and the circular component averages to zero over the bandpass.

Figs. 4.2(c) and 4.2(d) show the resulting nadir weighting functions for the magnetic equator and pole. The double peak in channel 2's weighting function over the pole results from averaging the two sides of the lines. As the antenna scans out from nadir, the weighting functions move up a few kilometers. Near the equator, this effect depends on whether one is looking along

the magnetic field or perpendicular to it, as in figs. 4.2(e) and 4.2(f) respectively. These are for the maximum scan position (43.2^{o}), in which the line of sight intersects the earth at an angle of 53.5^{o} from vertical, assuming an orbit altitude of 1100 km. Fig. 4.2(h) shows the 53.5^{o} weighting functions at the magnetic pole. Brightness temperatures corresponding to the weighting functions are listed in table IV-2. The large change from equator to pole (cases c vs. d, or e and f vs. h) is mostly due to the change in atmospheric temperature; a tropical model atmosphere was used to compute the equatorial weighting functions, and a 60^{o} latitude winter atmosphere for the polar weighting functions.

In a polar orbit, scanning crosswise to the spacecraft track, the lines are doppler shifted due to the projection of the earth's rotation along the line of sight. This effect is greatest at the equator, where it is 55 kHz for the maximum scan position. The weighting functions of fig. 4.2(f) have been recomputed in fig. 4.2(g) taking this small effect into account. It makes a difference of $\leq$ 0.4 K on the brightness temperatures as listed in table IV-2. Fig. 4.2(f) is actually not realistic to that extent, but we have computed it in order to isolate the effect of the frequency shift.

Two other possible sources of error are frequency drift of the radiometer local oscillators and inaccuracy in modeling the earth's magnetic field. According to Dr. R. Iwasaki of JPL, the first L. O. frequency changes by 3 kHz over the temperature range

Table IV-2. Brightness temperatures (K) corresponding to the weighting functions in fig. 4.2(a) - (h)

channel no.	a	b	c	d	e	f	g	h
1	211.4	210.2	210.8	248.1	205.9	200.4	200.7	242.5
2	248.1	253.9	251.0	245.8	244.8	244.5	244.1	244.8
3	262.4	262.7	262.6	249.9	260.9	261.1	261.1	253.0
4	261.3	261.2	261.3	243.3	263.3	263.4	263.4	247.8
5	256.3	256.3	256.3	235.9	260.0	260.0	260.0	240.3
6	251.8	251.7	251.8	230.8	255.9	255.9	255.9	235.0
7	242.5	242.5	242.5	223.1	246.9	246.9	246.9	226.3
8	232.3	232.3	232.3	217.4	236.6	236.6	236.6	219.4
9	214.0	214.0	214.0	214.2	218.6	218.6	218.6	213.9
10	277.9	277.9	277.9	246.3	267.1	267.1	267.1	240.9
11	258.2	258.2	258.2	236.5	245.2	245.2	245.2	229.5
12	218.9	218.9	218.9	218.4	211.7	211.7	211.7	216.5

0 to 50 C, and the second L. O. changes by 350 Hz. The respective accuracies of the frequencies are the same order of magnitude. The earth's magnetic field can be fitted to better than 1 % accuracy by a tenth-degree spherical harmonic expansion (Knecht, 1972). Both of these sources of error would thus be insignificant.

B. Temperature retrievals

To predict the potential of this experiment we have computed simulations based on 16 selected rocket soundings of the upper atmosphere made from Ascension Island during the year 1971. Such soundings are made more or less regularly by the Meteorological Rocket Network. Four of the stations in this network launch rockets that reach altitudes of 80 km or more at intervals of 2-8 weeks. We limit our analysis to one location and a vertical line of sight, although one of the major attractions of a satellite experiment, particularly if it is operated in a scanning mode, is its coverage of the entire globe.

For the purpose of computation, we divide the atmosphere from 0.002 mb to 1000 mb into 90 layers, equally spaced along the logarithm of pressure. Each layer is therefore approximately 1 km thick. The brightness temperature $(T_B)_i$ observed by channel i may be expressed as

$$(T_B)_i = \sum_j W_{ij} T_j + e_i \qquad (4.1)$$

where T_j is the temperature of level j, and e_i is the error of the measurement resulting from noise. The weighting functions W_{ij} for the nine channels are computed for the magnetic latitude of Ascension Island (-15^{o}).

It would be of interest to recover an actual temperature profile, as well as the weighted temperatures (brightness temperatures). A minimum mean-square error estimate of the temperature profile (Foster, 1961; Rodgers, 1971) is given by

$$\underline{T}^* = \underline{\underline{D}}(\underline{T}_B - \langle \underline{T}_B \rangle) + \langle \underline{T} \rangle. \tag{4.2}$$

where

$$\underline{\underline{D}} = \underline{\underline{C}}_T \underline{\underline{W}}^t [\underline{\underline{W}} \underline{\underline{C}}_T \underline{\underline{W}}^t + \underline{\underline{C}}_e]^{-1} \tag{4.3}$$

and $\underline{T}^*$ is the vector of estimated atmospheric temperatures, $\underline{\underline{C}}_T$ is the covariance matrix of atmospheric temperatures, and $\underline{\underline{C}}_e$ is the covariance matrix of measurement noise (normally diagonal). Angle brackets denote the mean, and superscript t the transpose. A difficulty arises, however, because of the small number of soundings (16) available to compute $\underline{\underline{C}}_T$. Equations 4.2 and 4.3 constitute a linear regression with each channel contributing an independent variable. Since the means are removed from the variables, the set would have only 16 - 12 - 1 = 3 degrees of freedom remaining, so the results would be meaningless. Since we are presently concerned primarily with the stratosphere and mesosphere, we might use only channels 1-9 in the simulation,

giving 6 degrees of freedom. This is still too few to produce reliable results. We may, however, use eq. 4.3 to obtain a lower bound on the errors that we could obtain by using any inversion method, since by definition it produces minimum errors for the given set of soundings.

If we make the ad hoc assumption that

$$\sum_j (C_T)_{ij} W_{kj} = 2n\sigma_T^2 W_{ki}, \tag{4.4}$$

where n characterizes the number of layers over which correlations persist, and σ_T is an assumed a priori standard deviation of temperature, then we obtain a "minimum information" solution (Foster, 1961)

$$\underline{\underline{D}} = \underline{\underline{W}}^t [\underline{\underline{W}}\underline{\underline{W}}^t + \frac{1}{2n\sigma_T^2} \underline{\underline{C}}_e]^{-1}. \tag{4.5}$$

Typical values of 2n are 6-10 (i.e., a vertical correlation length of 3-5 km) which is less than the widths of the weighting functions. The correlations between channels that are implied by eq. 4.5 are therefore induced by the overlap of the weighting functions rather than by the statistics of the atmosphere. Thus we are neglecting all correlations between layers that are separated by more than the width of the weighting functions. For this reason our results using eq. 4.5 will be somewhat suboptimum, but we are dependent on a priori statistics only for the mean profile. For these computations we used $2n\sigma_T^2 = 200\ K^2$.

The residual errors obtained when this inversion method is

applied to the Ascension Island soundings are shown in fig. 4.3 by the line labeled B, along with the a priori standard deviation labeled A. The minimum mean-square error solution (statistical) is shown by the line labeled C. (It should be noted that these computations used our earlier specification of the 7^- and 9^- lines; however, only channels 8 and 9 are significantly affected). We see that both solutions leave residuals of 2-3 K in the stratosphere, but 4 K or more in the mesosphere. One cause of this is certainly the greater width of the weighting functions for channels 1 and 2; atmospheric structure that is finer than the weighting functions cannot be recovered, and therefore contributes to the residuals. This problem is illustrated by fig. 4.4, which shows correlation coefficients

$$\rho_{ij} = (C_T)_{ij} \left[(C_T)_{ii}(C_T)_{jj}\right]^{-\frac{1}{2}} \qquad (4.6)$$

as a function of j, for selected values of i. The temperature at any level is highly correlated with other levels for only a few km above and below, and somewhat less near the tropopause and stratopause. Our stratospheric weighting functions are only slightly wider than these correlation functions, but the mesospheric channels (1 and 2) have weighting functions about twice as wide as the others. Consequently a large part of their variation in brightness temperature is produced by uncorrelated levels of the atmosphere. When one attempts to invert the radiative transfer equations, and solve for temperature at a specific level, the

result is predictably disappointing. Possibly the soundings, which are known to possess poor reliability above 65 km, also introduce a form of noisiness in the temperature profile that is not genuine, but it is difficult to determine the extent to which this might be true.

The sharpness of the weighting functions is determined by the rate of change of the absorption coefficient with height (Poon, 1974). In the line wings, the absorption goes as P^2. For channels 1 and 2, on the other hand, the pressure dependence of absorption is less. (The weighting function for channel 2 is also broadened by having a bandwidth comparable to its distance from the center of the line; different frequencies within the bandpass have weighting functions that peak at appreciably different heights.) Since the pressure dependence of the absorption coefficient is determined by the spectroscopic properties of oxygen, this appears to be a fundamental limitation on the accuracy of temperature retrievals in the 50-80 km range from a down-looking measurement.

In summary, we may distinguish three regions of the atmosphere with respect to temperature profile retrievals. Up to 50 km (1 mb) the weighting functions are sufficiently narrow to recover most of the profile structure; rms errors of 2-3 K are predicted. The minimum information method does nearly as well as the optimum statistical method. In this region atmospheric statistics are plentiful, and could be used to obtain a slight improvement over the minimum information method. Since we considered only one location, in the tropics, in fig. 4.3, the a priori variation is smaller

than for the entire globe. Thus the actual reduction in variance provided by the sounder would be greater than implied by the figure. From 50 km to 75 km (0.02 mb) the weighting functions are wider and less detailed information about the profile is obtained. Atmospheric statistics are scarce above 60 km, limiting use of the statistical inversion method there. The region above 75 km is penetrated only by the tails of the weighting functions and no useful information is obtained.

C. Discussion of algorithms for data reduction

For a space experiment we are faced with the task of interpreting data taken over the entire earth, at several scan angles. An inversion method that does not require a priori statistics is preferred. The minimum information solution is probably the simplest and most economical of computer time, since the matrix inversion is done ahead of time, and the operational data reduction algorithm is essentially a matrix multiplication. Iterative methods such as those of Chahine (1968) and Smith (1970) might also be considered, but they involve more computation.

There are three variables that affect the weighting functions appreciably: scan angle; magnetic latitude; and the azimuthal angle between magnetic north and the line of the scan, projected on the earth. The last is most important near the equator. Referring to table IV-2 and comparing cases e and g, we see that it makes a difference of $\sim$5 K for channel 1, less than 1 K for channel 2, and negligable differences for the other channels.

Therefore we can adequately account for this effect by making a correction to the brightness temperatures. Since the magnetic latitude moves the weighting functions for channels 1-3 by rather large amounts, it would best be treated by computing separate $\underline{D}$ matrices for perhaps 5 fixed latitudes and interpolating. For 7 scan positions (nadir and 6 on either side), 35 matrices are required. Each matrix has 90 x 12 = 1080 elements, so the total is 38 K words, rather large but manageable.

Worth noting is the fact that only channels 1-3 are appreciably affected by the magnetic field. If the cost of inverting all of the data up to 80 km altitude were to prove prohibitive, the profile to 50 km could be retrieved from channels 4-12 with no more complexity (except for the larger number of channels) than encountered with the Nimbus-F SCAMS, and with very similar programs.

V. Summary and Conclusions

A. Scientific Results

The theoretical microwave transmittance functions for oxygen were significantly improved by incorporation of coherence effects between overlapping spectral lines. This approach, described in chapter III, differs in principle from the models of Meeks and Lilley (1963) and Reber (1972) which summed lines incoherently. Laboratory measurements in the pressure range 100-400 mb (Poon, 1974) confirm the coherent model, and measurements from aircraft and ground stations, described here in chapter II, are also consistent.

In the course of the experimental program we measured for the first time the 23_-, 25_-, 29_- and 31_- atmospheric oxygen lines and measured the frequencies of several such lines with improved precision. The polarization and Zeeman splitting of the 27_- line were also measured. On the basis of these measurements we conclude that the microwave spectrum of oxygen is sufficiently well understood to justify a space experiment that would use strong oxygen lines to sound the atmospheric temperature profile up to $\sim$75 km. The principal remaining uncertainty in the oxygen spectrum concerns the collisional line widths for large N values, which presently are extrapolated from measurements at N = 3 to 9. These latter measurements are nonetheless quite appropriate for the proposed satellite experiment employing the 5_+ and 7_- resonances.

Calculations of the effects of the terrestrial magnetic field

and instrument viewing angles suggest that they are quite important considerations in retrieval of temperature profiles from radiance data, but that they can be incorporated in the retrieval process in a manageable fashion. The rms retrieval accuracy for temperature profiles 0-50 km is estimated to be ∿2-3 K, but slightly worse at 50-75 km due to the broader weighting functions there. The microwave temperature sounder (MTS) has three important advantages relative to comparable infrared sensors; 1) much less sensitivity to clouds, 2) altitude coverage 0 to 75 km, and 3) narrower weighting functions, particularly at stratospheric and mesospheric altitudes. These advantages make MTS attractive for both research and operational objectives.

B. Proposed Satellite Missions

Two applications of the MTS system appear particularly attractive; 1) replacement of the Tiros-N operational meteorological satellite microwave sounder MSU with the improved MTS, and 2) flight on space shuttle missions together with other atmospheric sounding experiments, particularly those sounding stratospheric and mesospheric temperature profiles.

The replacement of the 4-channel Tiros-N MSU with the 12-channel MTS would modestly increase the size, weight, power, and data requirements, but to an extent comfortably within the present growth capability of the Tiros-N satellite. The weight would increase from 47.3 to 52 pounds, power from 29 to 42 watts, and size from 6 x 8 x 13, 6 x 9 x 6.5, and 9 x 7 3/4 x 15 inches to

6 x 13 x 13, 6 x 11 x 6.5, and 9 x 7 3/4 x 15 inches for the instrument, power supply, and antenna modules, respectively. The engineering model is presently being fabricated at the Jet Propulsion Laboratory, and timely fabrication of flight units appears practical. The Tiros-N application requires a window channel for sensing the terrestrial surface and so channels 10, 11, and 12 should be shifted slightly in frequency to duplicate channels 1, 2, and 3 of MSU, respectively. Channel 4 of the MSU would then be replaced by channel 9. Channel 9 now peaks above 20 km, but by using the 11_ and 13_ lines it could be lowered to 16 km, or to other altitudes for other line pairs. Lowering channel 9 several kilometers will lower the altitudes of channels 1-8 by comparable amounts, which would be quite appropriate for the Tiros-N mission. Such shifts in line frequencies involve no engineering difficulties.

Flight of MTS on space shuttle missions could also be a valuable precursor to future versions of the Tiros-N microwave sounder unit, if not incorporated earlier, or be a precursor for such instruments on future space stations for continuous synoptic observations and climatic assessment.

The space shuttle will also carry other sensors for monitoring the stratosphere and mesosphere, and the MTS would be a valuable part of such combined limited-duration experiments. No satellite instrument now duplicates the altitude coverage of the MTS, and so its unique temperature - sensing characteristics make it a valuable satellite system for atmospheric sensing.

REFERENCES

Anderson, B. G., S. M. Thesis, M. I. T., Cambridge (1973).

Barrett, A. H., and K. S. Lam, RLE Progress Report No. 115, M. I. T. Research Lab. Electronics, Jan. 1975, pp. 74-83.

Chahine, M. T., J. Opt. Soc. Amer. 58, 1634 (1968).

Dillon, T. A., and J. T. Godfrey, Phys. Rev. A 5, 599 (1972).

Foster, M. J. SIAM 9, 387 (1961).

Gardiner, W. C. Jr., H. M. Pickett, and M. H. Proffitt, J. Chem. Phys., in press (1975).

Gordon, R. G., J. Chem. Phys., 45, 1649 (1966).

Gordon, R. G., J. Chem. Phys. 46, 448 (1967).

Kaufman, I. A., Ph.D. thesis, Columbia Univ., New York (1967).

Knecht, D. J., A Revision of Ch. 11 of Handbook of Geophysics and Space Environments, AFCRL-72-0570, pp. 39-43 (1972).

Lenoir, W. B., J. App. Phys. 38, 5283 (1967).

Lenoir, W. B., J. Geophys. Res. 73, 361 (1968).

Liebe, H. J., IEEE Trans. Micro. Th. Tech. MTT-23, 380 (1975); also Studies of oxygen and water vapor microwave spectra under simulated atmospheric conditions, Office of Telecommunications Report, June 1975.

Maryott, A. A., and G. Birnbaum, J. Chem. Phys., 32, 686 (1960).

Meeks, M. L., and A. E. Lilley, J. Geophys. Res., 68, 1683 (1963).

Mingelgrin, U., Ph.D. thesis, Harvard Univ., Cambridge (1972).

Mizushima, M., and R. M. Hill, Phys. Rev. 93, 745 (1954).

Pickett, H. M. J. Chem. Phys., in press (1975).

Poon, R. K. L., Sc.D. Thesis, M. I. T., Cambridge (1974).

Reber, E. E., J. Geophys. Res., 77, 3831 (1972).

Rodgers, C. D., J. Quan. Spec. Rad. Tr. 11, 767 (1971).

Rosenkranz, P. W., IEEE Trans. Ant. Propag., AP-23, July 1975.

Smith, W. L., Appl. Opt. 9, 1993 (1970).

Waters, J. W., Ph.D. thesis, M. I. T., Cambridge (1970).

Waters, J. W., Nature 242, 506 (1973).

Welch, W. M., and M. Mizushima, Phys. Rev. A 5, 2692 (1972).

Wilheit, T. T., Jr., Ph.D. thesis, M. I. T., Cambridge (1970).

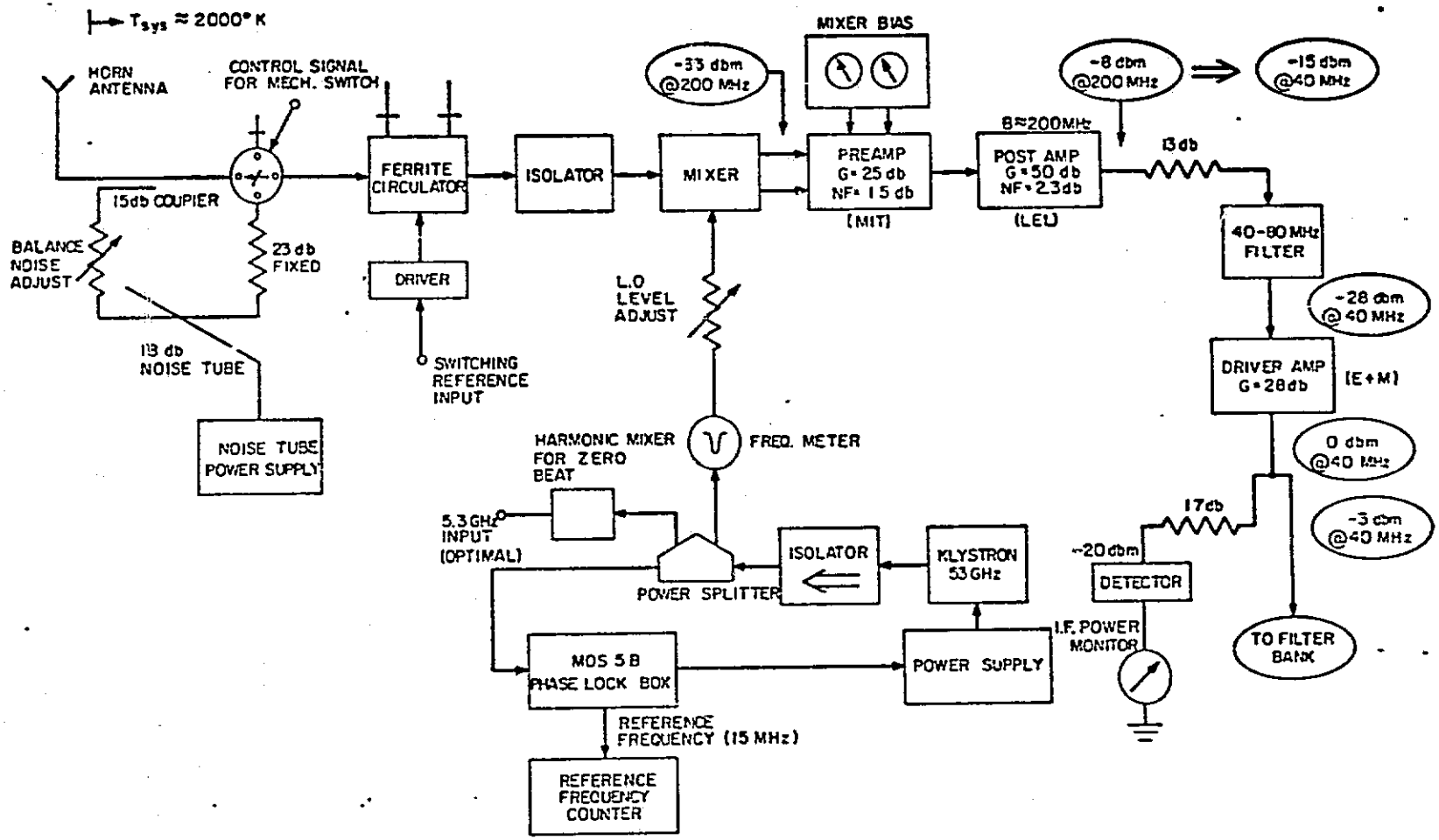

Figure 2.1 Block Diagram of Radiometer

2.2 Radiometer and phase-lock box mounted in a tiltable box.

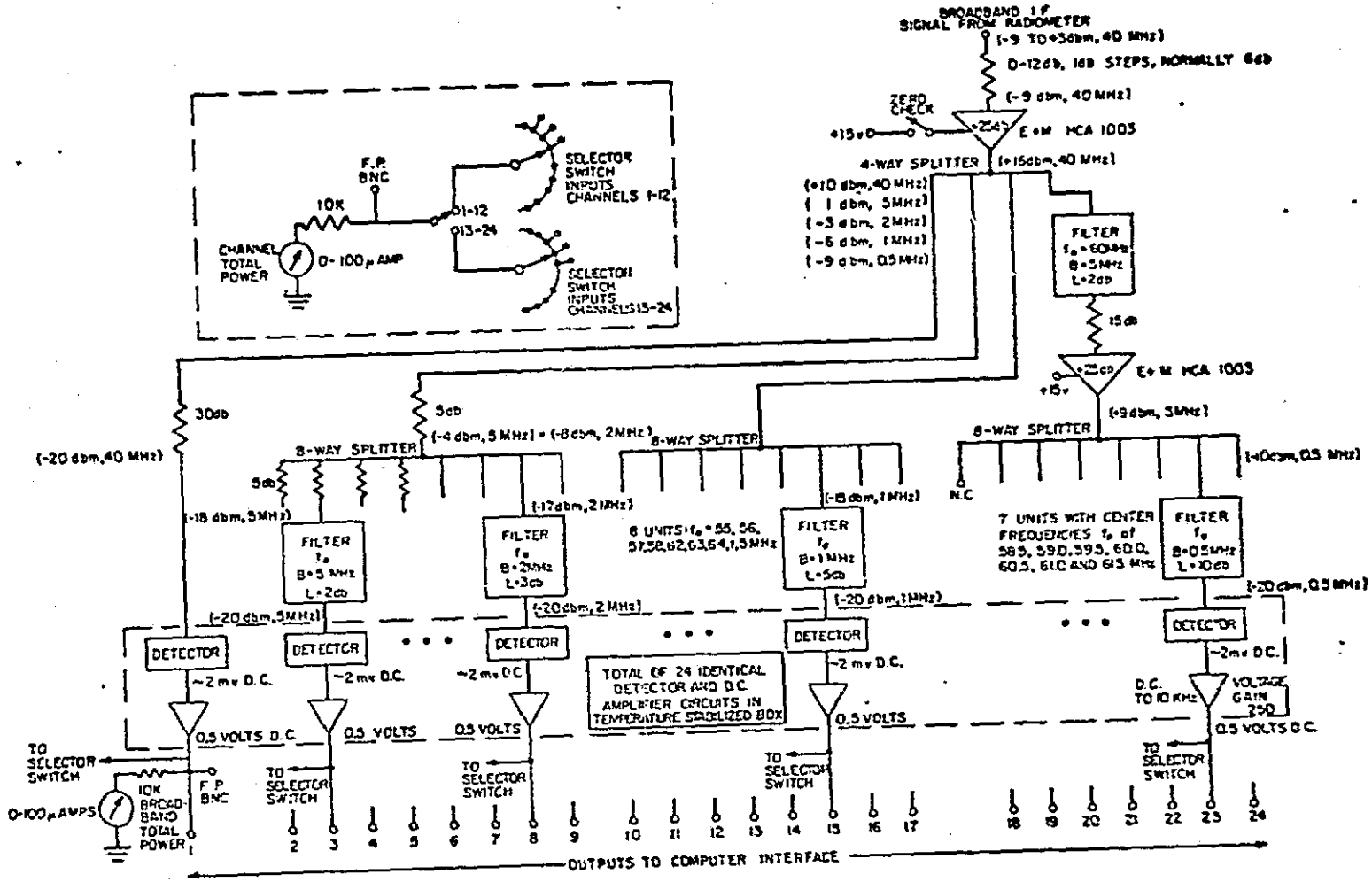

Figure 2.3 Filter Bank Block Diagram

2.4 Filter bank, data processor, and magnetic tape recording system.

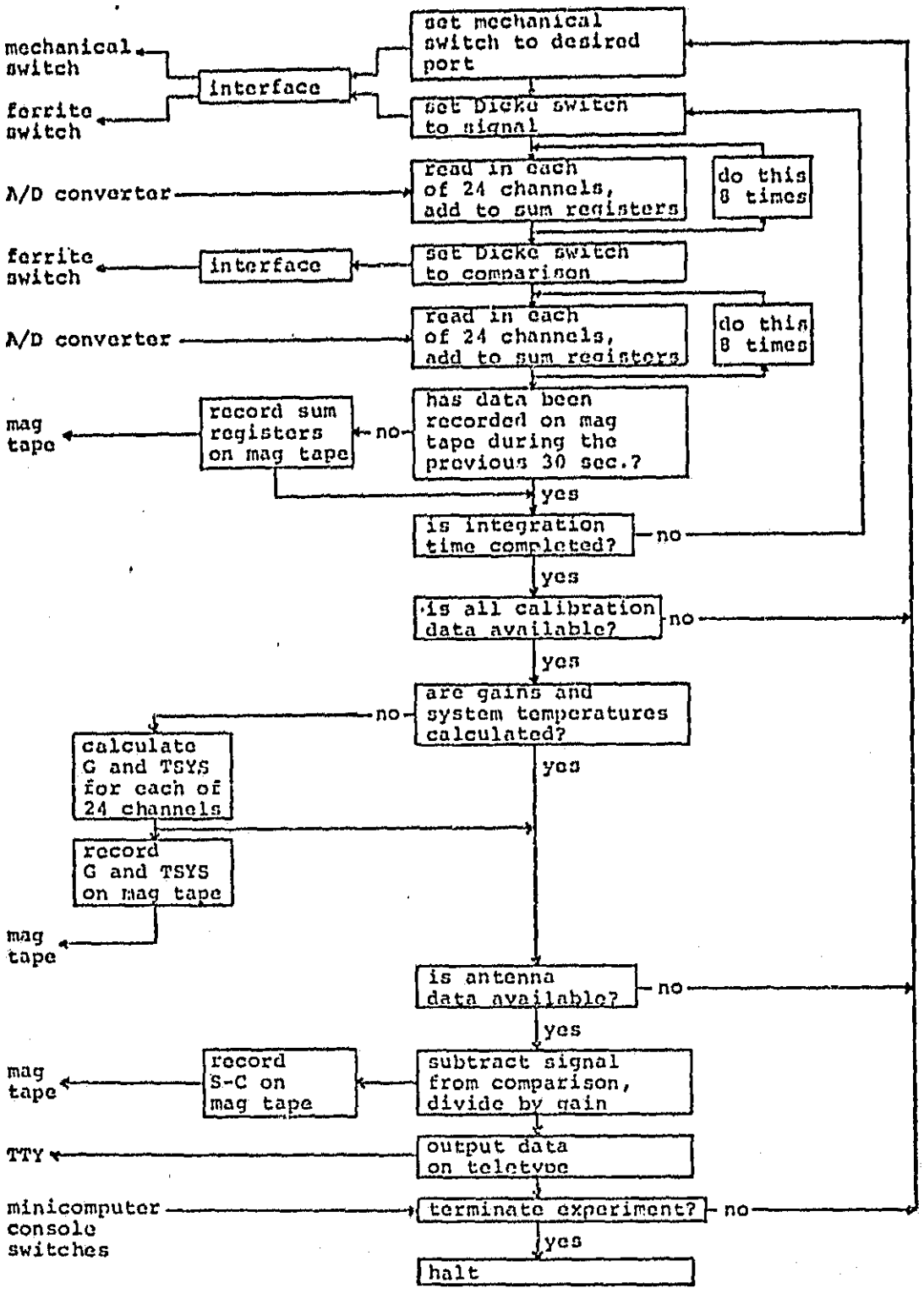

Figure 2.5 Block Diagram of NOVA Software

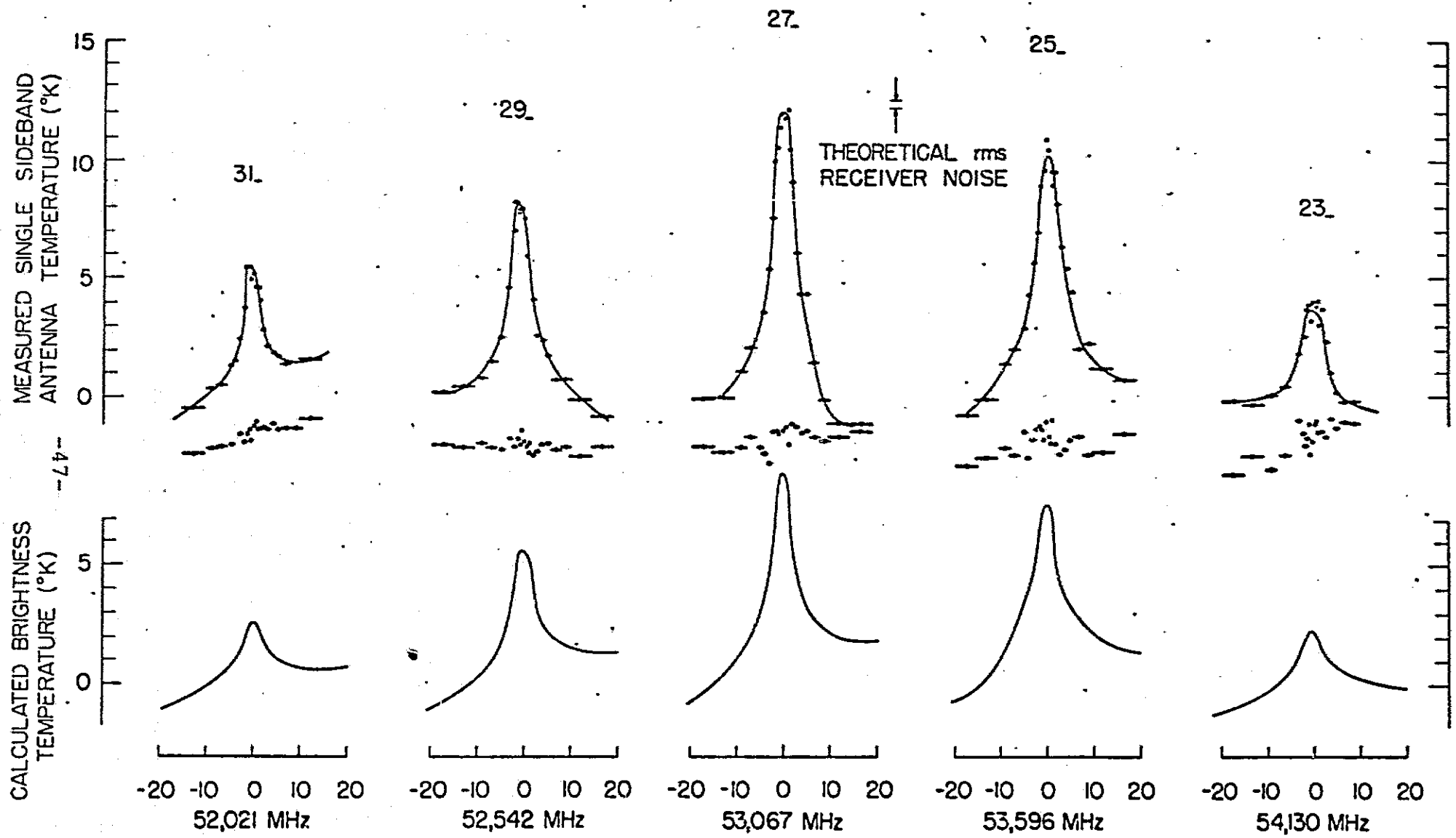

2.6 Measured (upper) and calculated (lower) atmospheric zenith emission. Each measured line and the instrumental baseline shown beneath,it represent integration for 16 min. The measurements were made during the week of August 30, 1972 at Haystack Observatory.

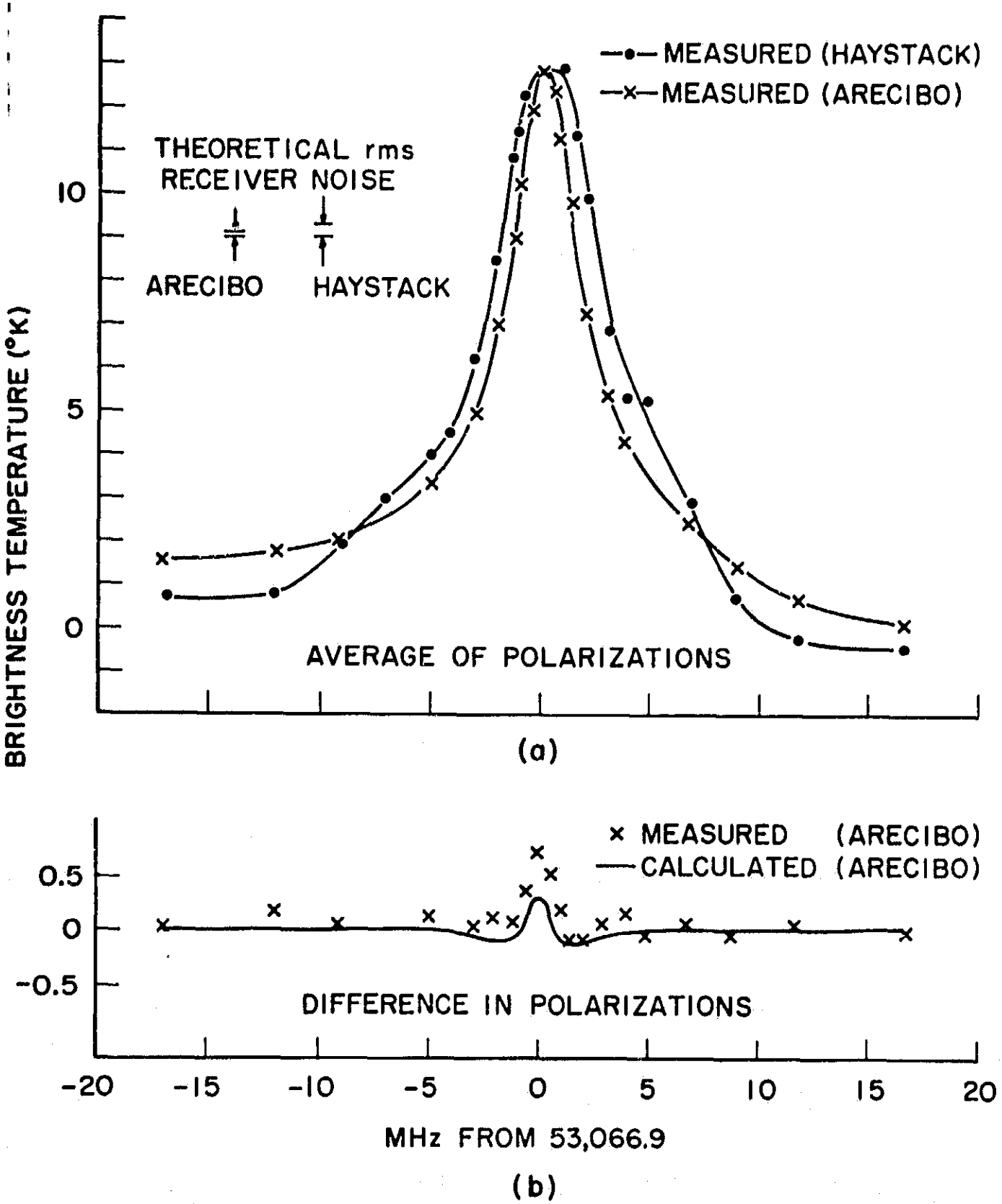

2.7(a) Atmospheric zenith emission by the 27_ O_2 line as measured on August 30, 1972 from Haystack Observatory (magnetic latitude 55°) and on November 1, 1972 from Arecibo Observatory (magnetic latitude 29°).

(b) Polarization of the 27_ O_2 line for Arecibo. The linear polarization in the magnetic east-west direction is stronger than in the magnetic north-south direction.

2.8 High-resolution measurements of the 27 O_2 line zenith emission made with the Haystack and Arecibo correlators on August 30 and November 1, 1972, respectively. The measurements average two orthogonal linear polarizations. Calculations which linearly sum the absorption by the various O_2 lines are also given.

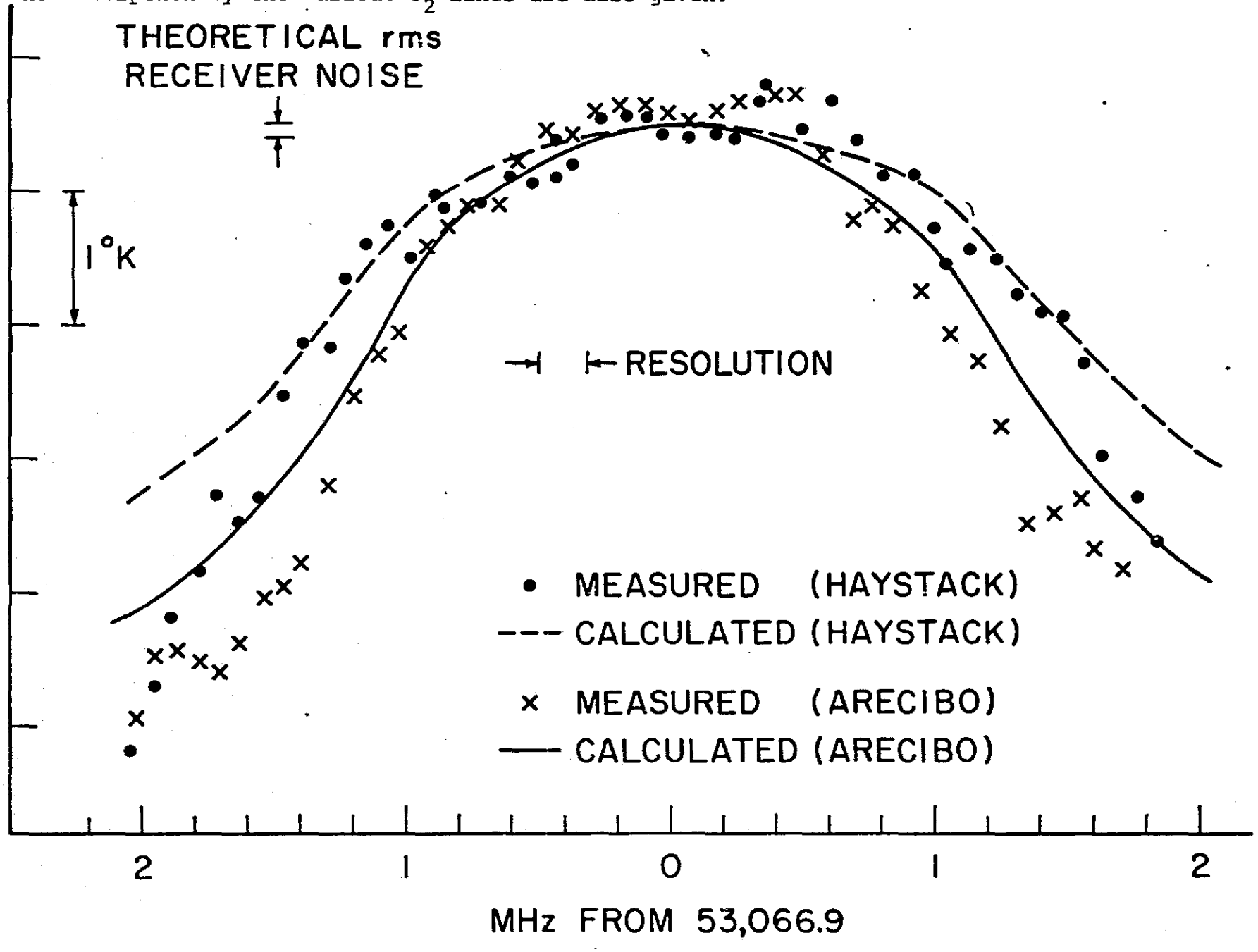

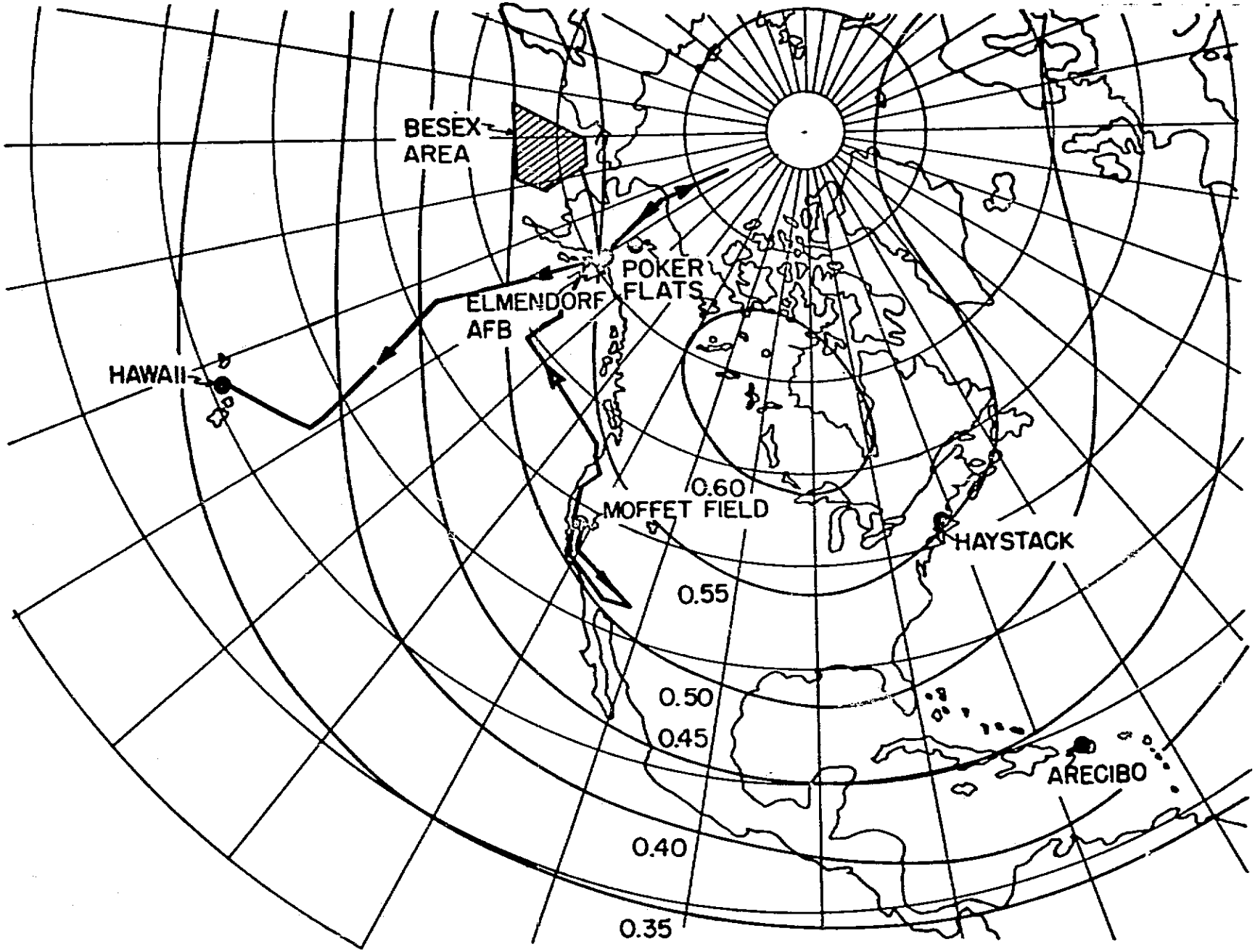

2.9 BESEX flights. Contours of the earth's magnetic field are also shown.

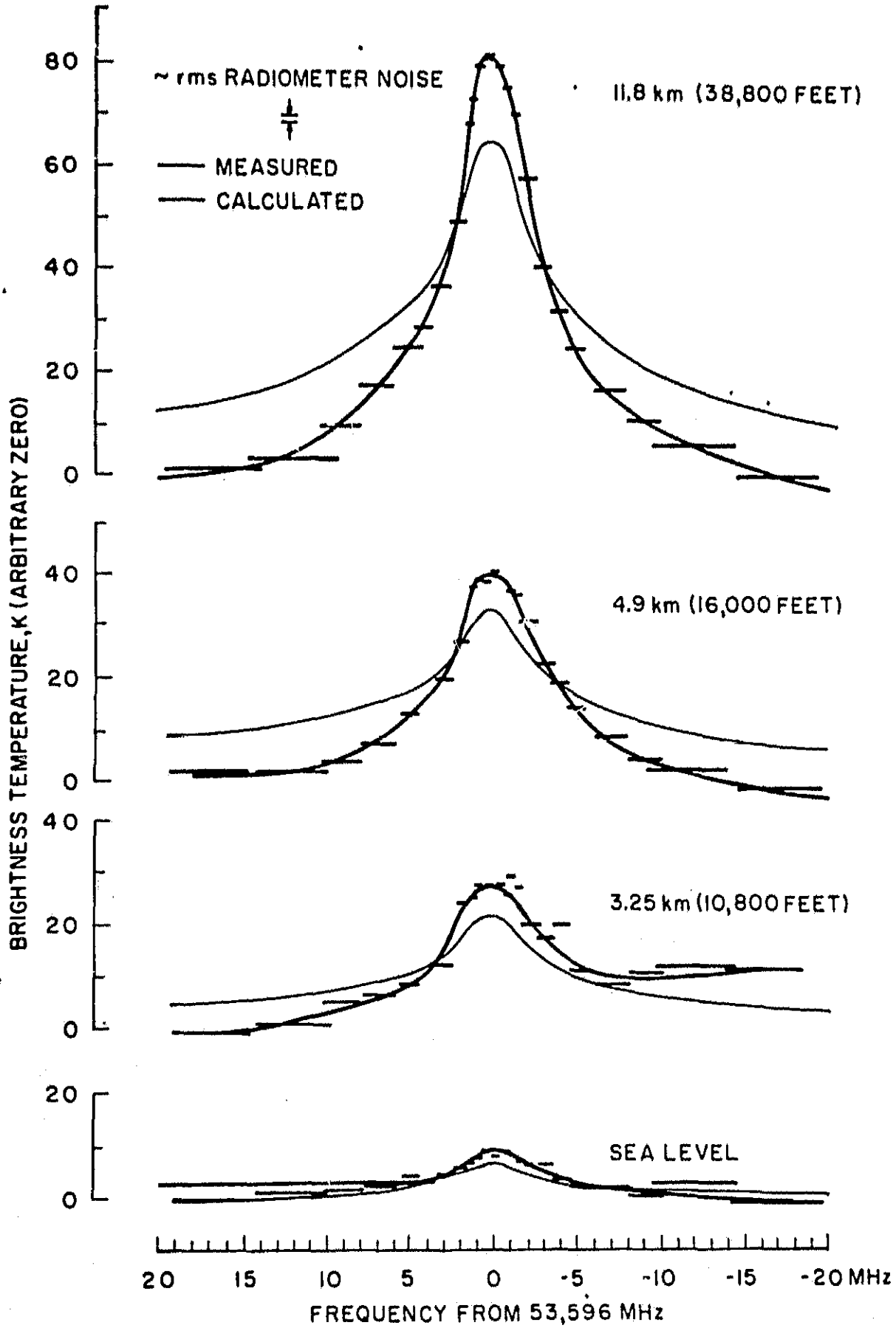

2.10 Line brightness variation with altitude over southwestern U. S., 8 February 1973.

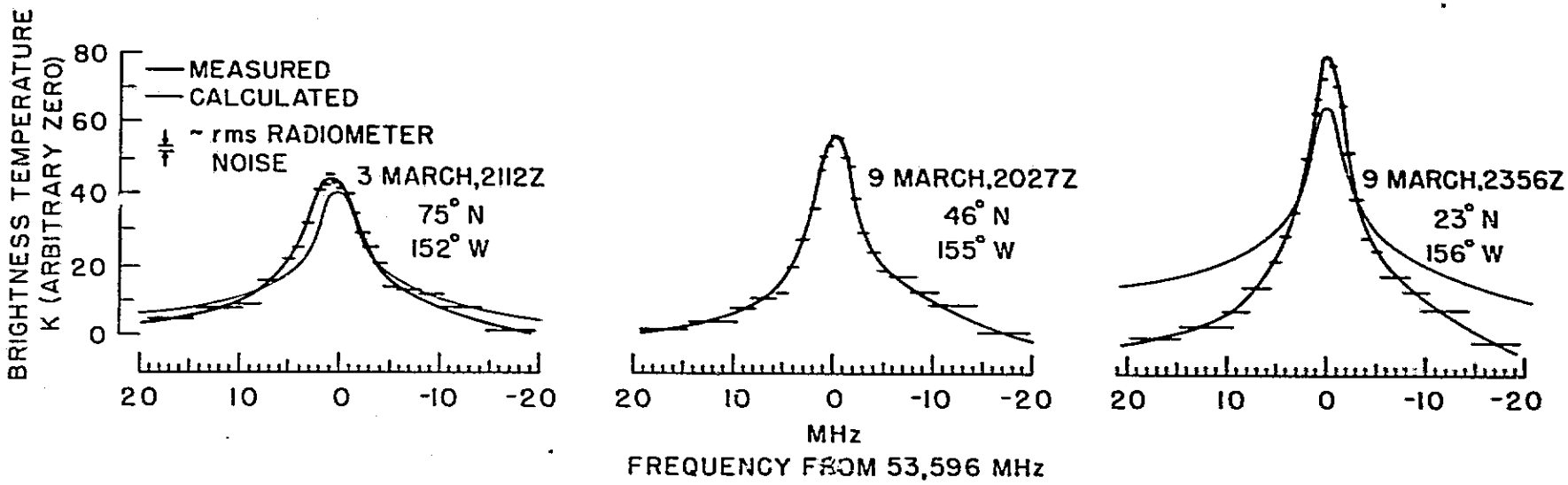

2.11 Line shape variation with latitude.

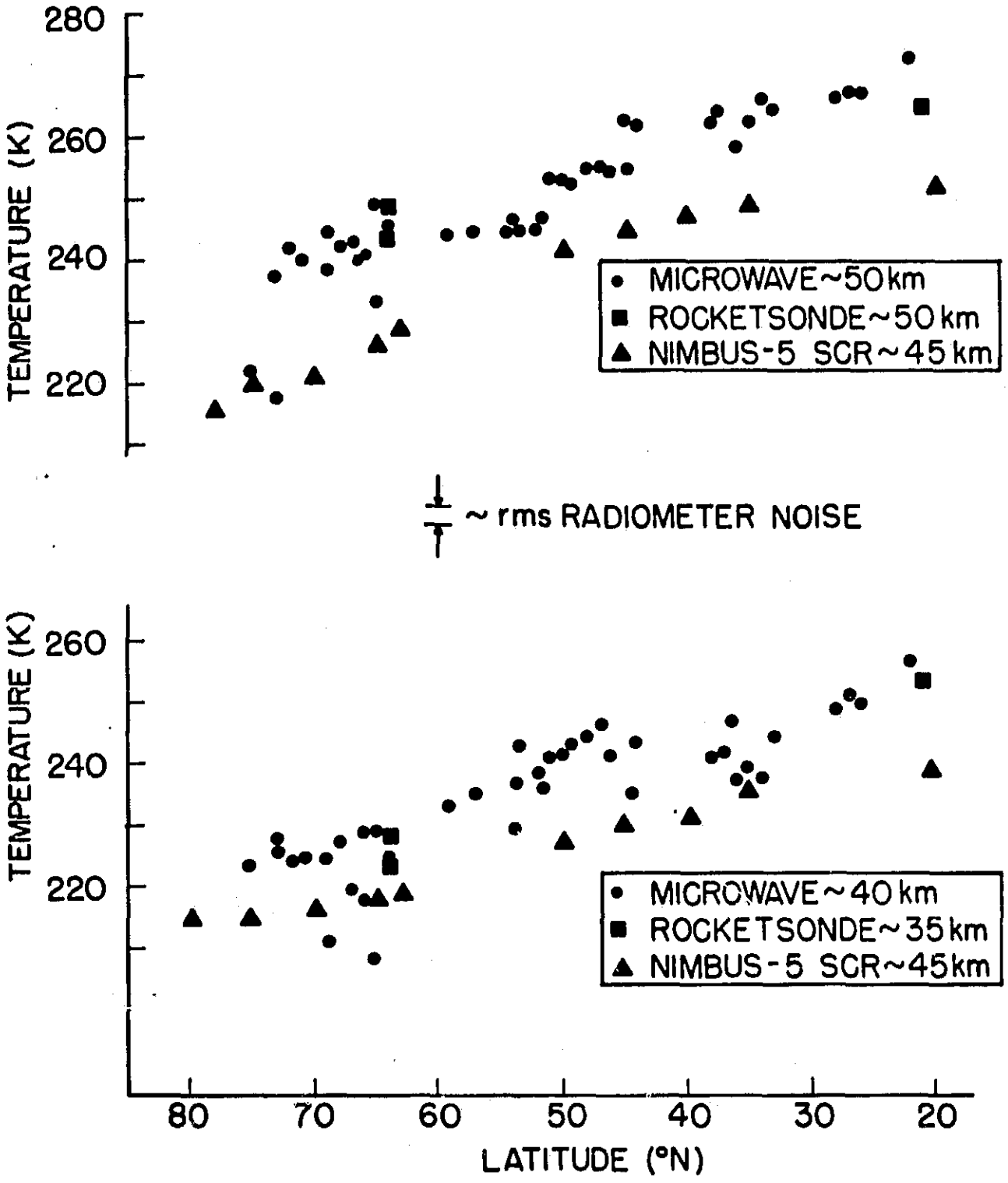

2.12 Comparison of stratospheric temperatures inferred from line measurements with rocketsonde and satellite measurements on 9 March 1973.

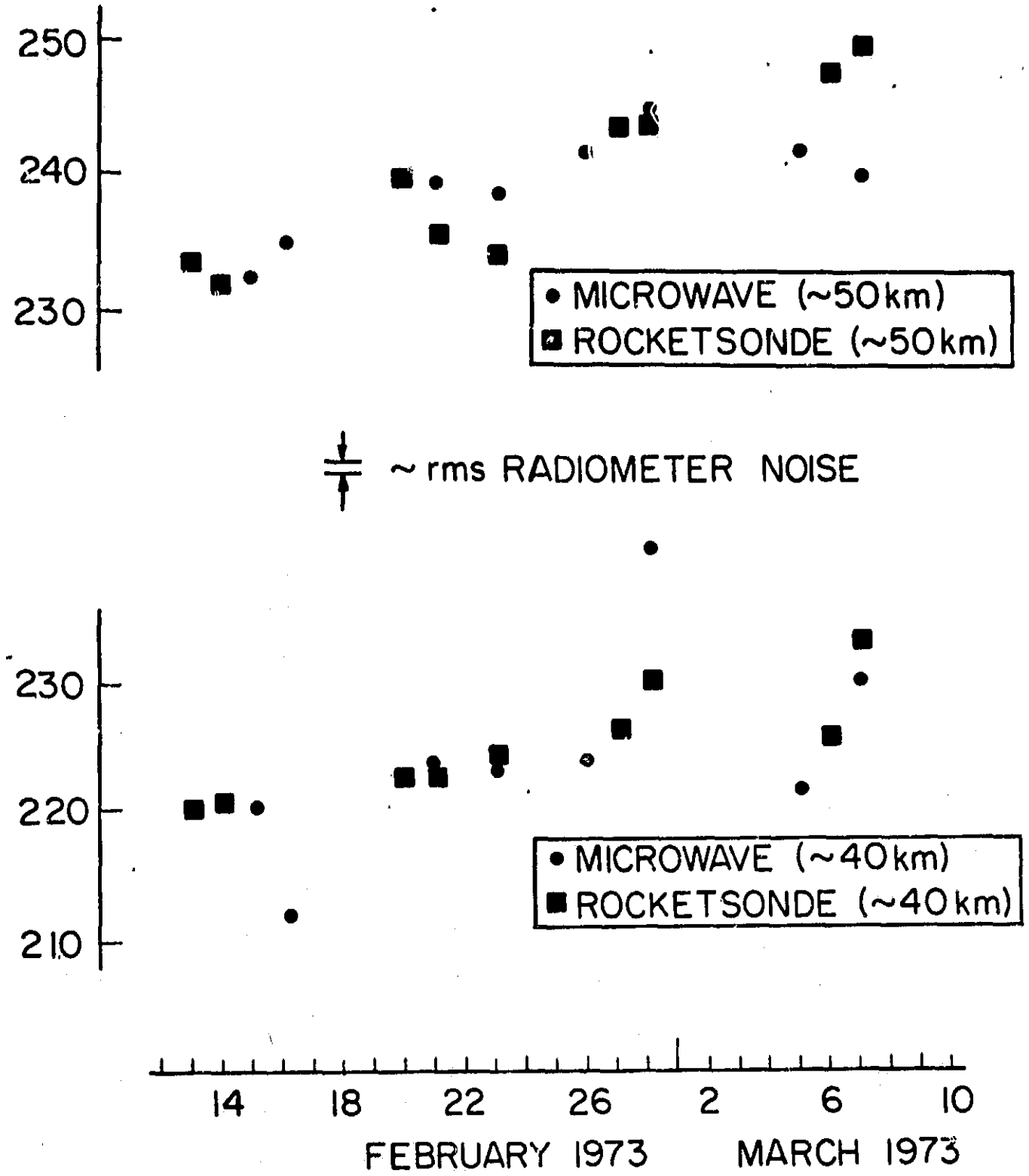

2.13 Comparison of stratospheric temperatures inferred from line measurements with rocketsonde measurements in Alaska.

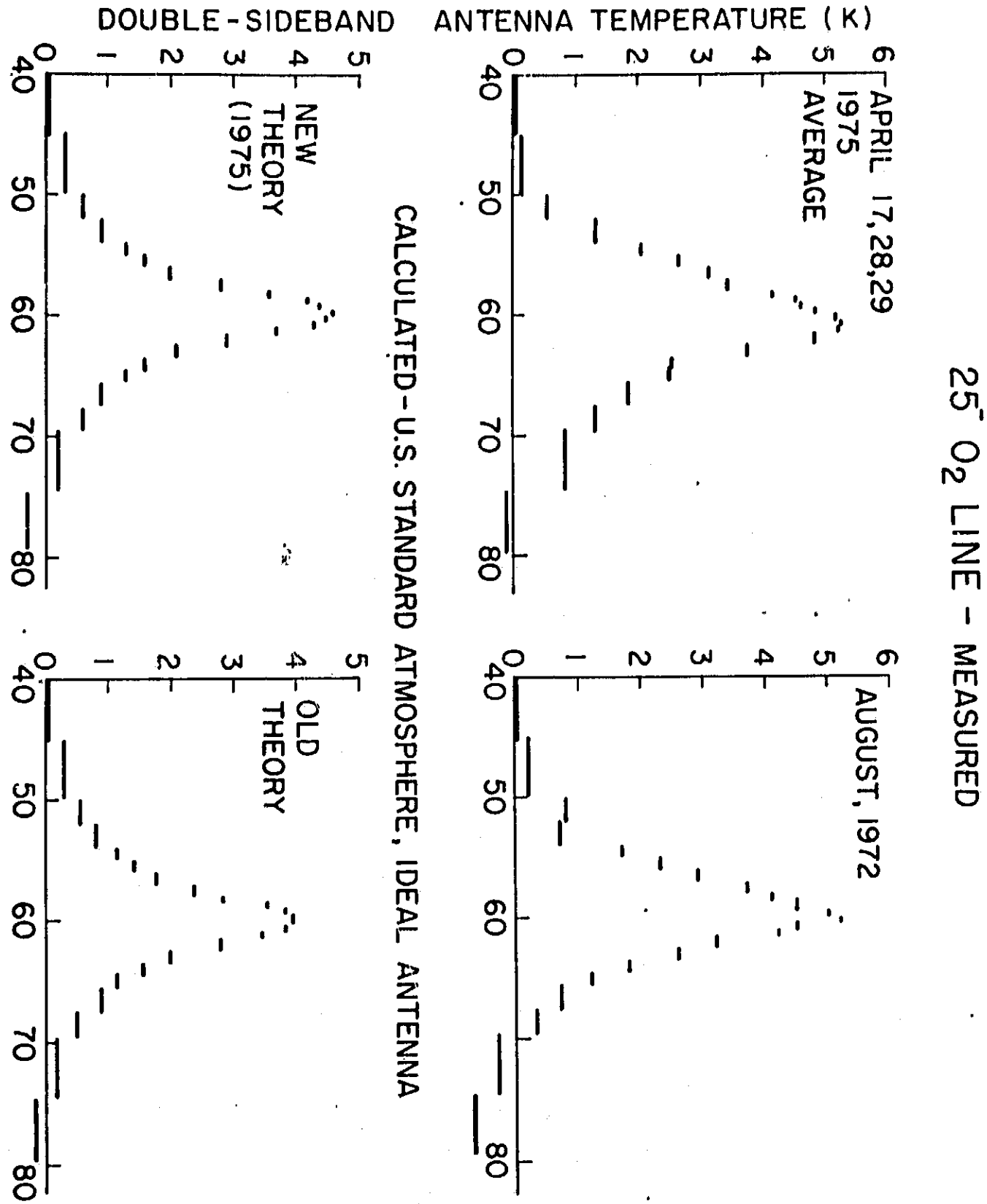

2.14 The 25¯ oxygen line observed from the M. I. T. campus, with two theoretical calculations. The antenna is pointed at zenith and the line is in the lower sideband of the radiometer.

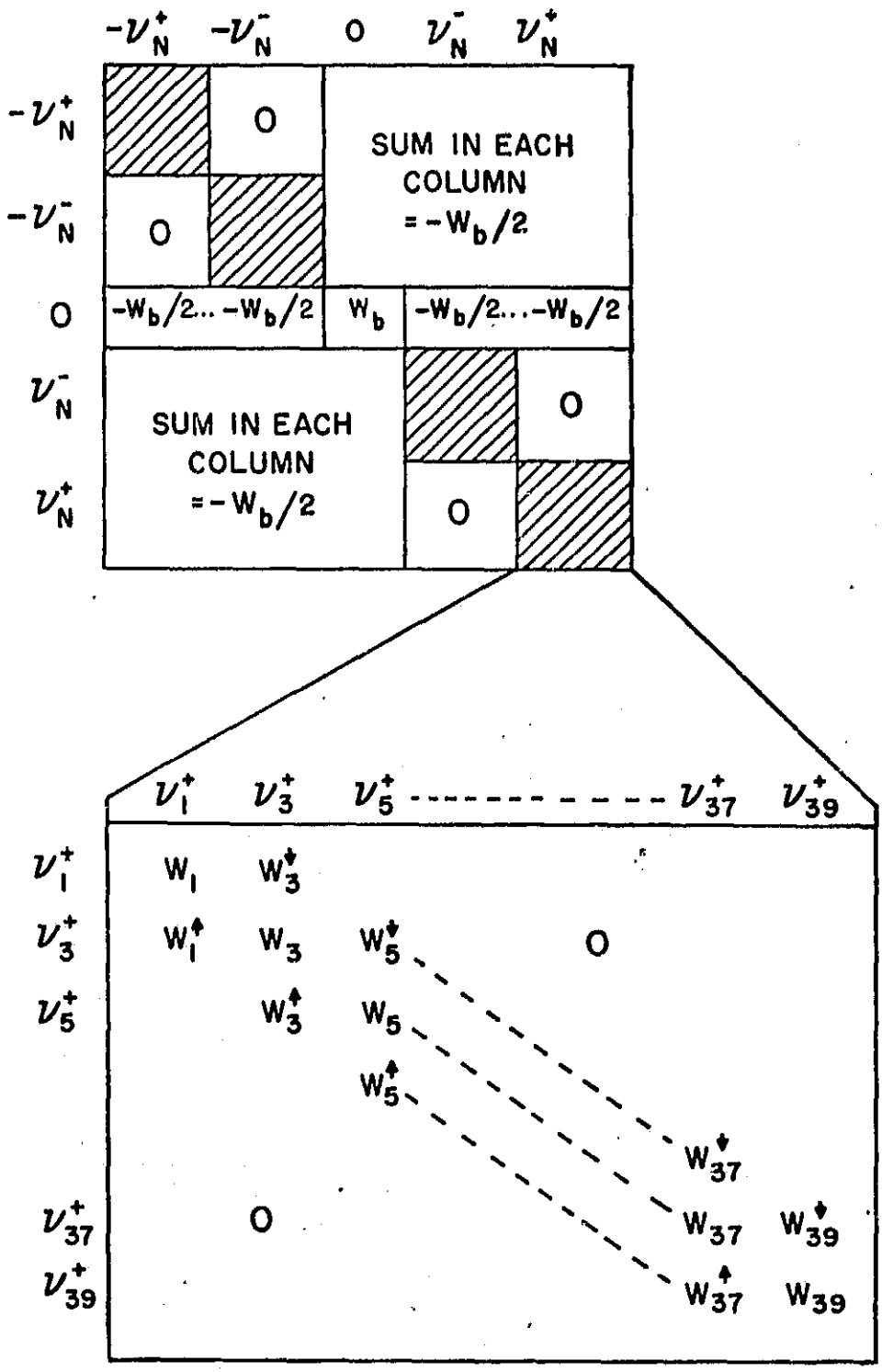

3.1 The W matrix. Elements associated with the zero frequency lines have been merged. The four shaded submatrices are alike.

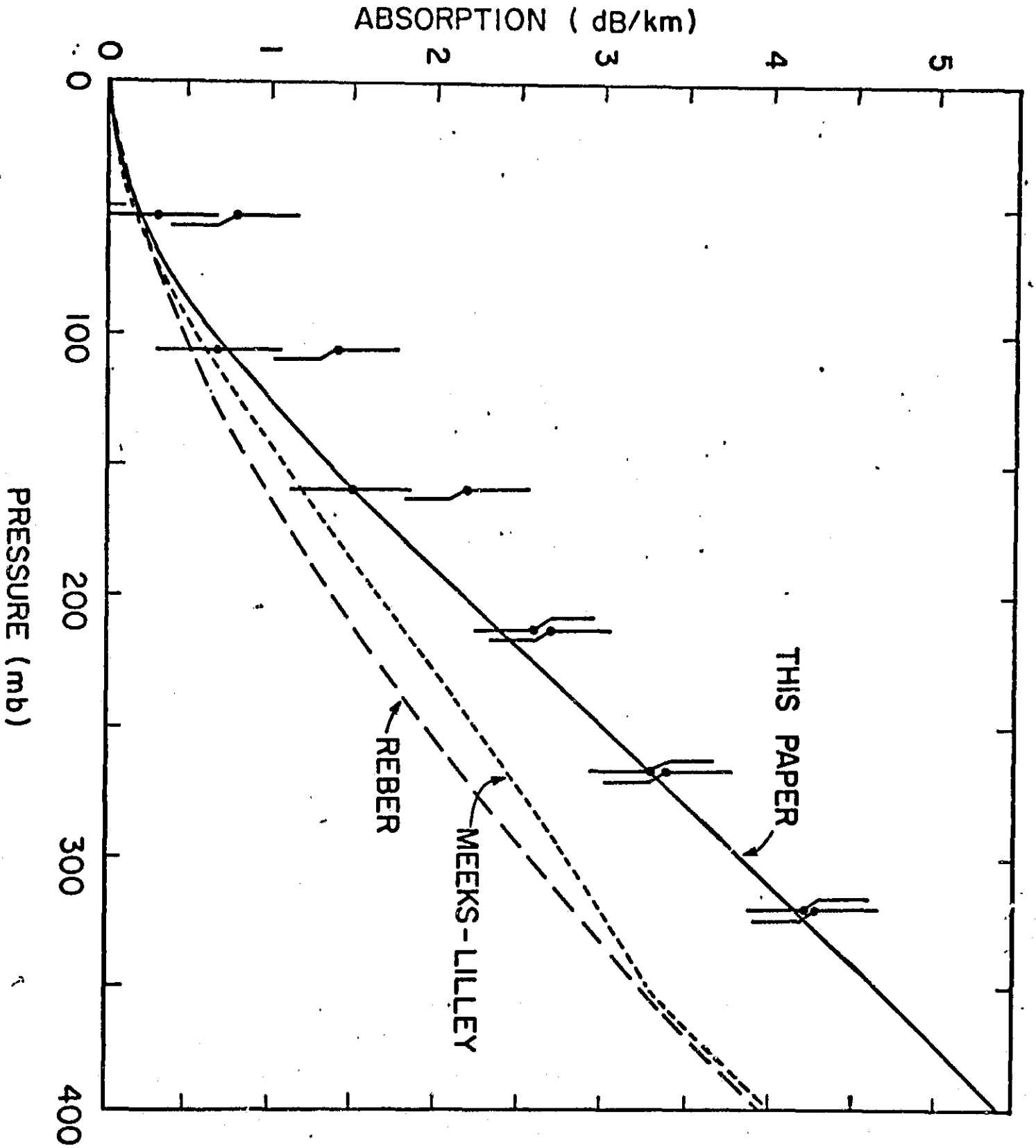

3.2 Absorption in dry air at 58.82 GHz and 295 K, computed for three models. Measurements are by Poon (1974).

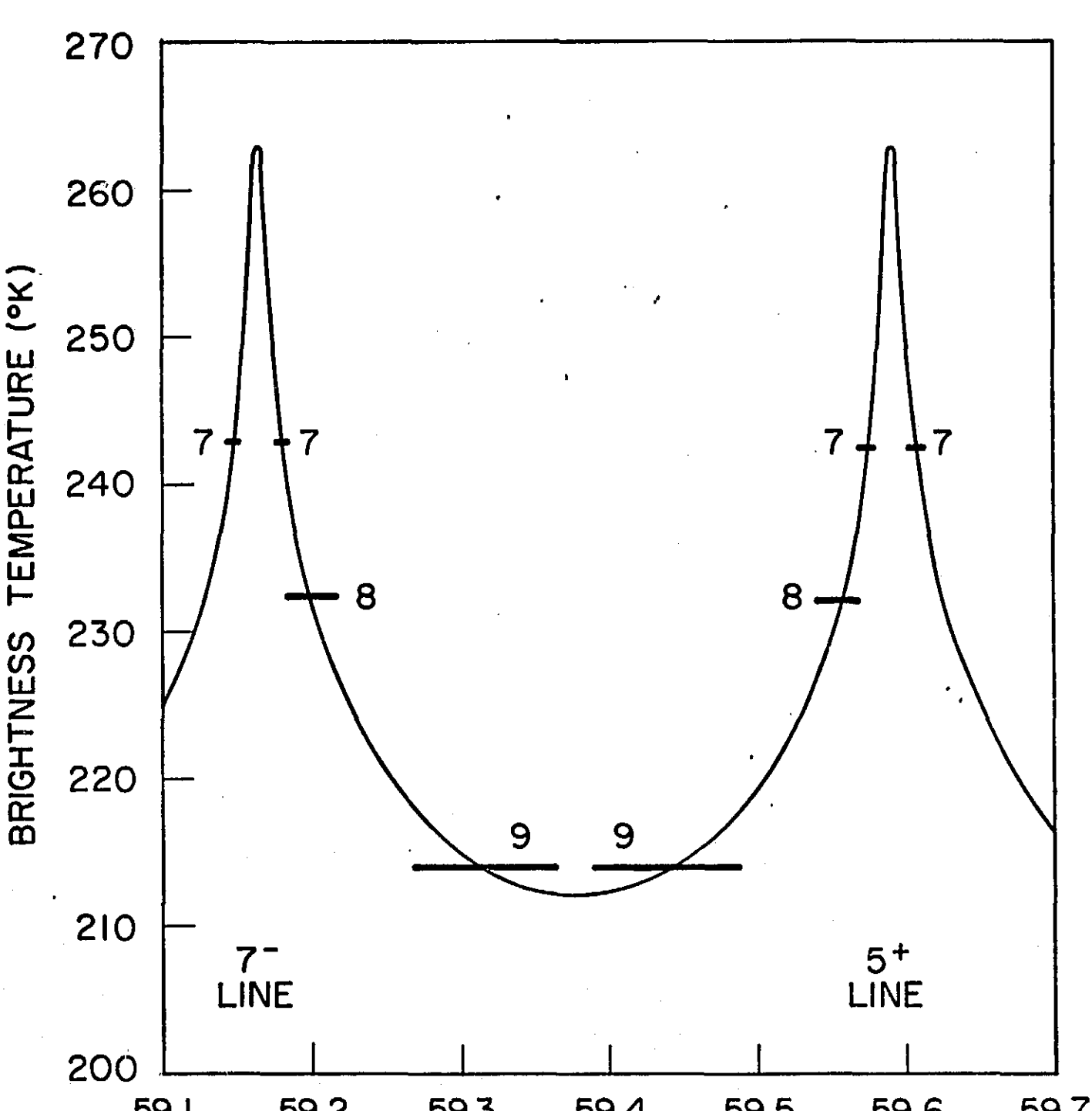

4.1(a) Brightness temperature spectrum near the 7^- and 5^+ lines looking downward at nadir over the magnetic equator, showing positions of the instrument sidebands. Each sideband is labled with its channel number.

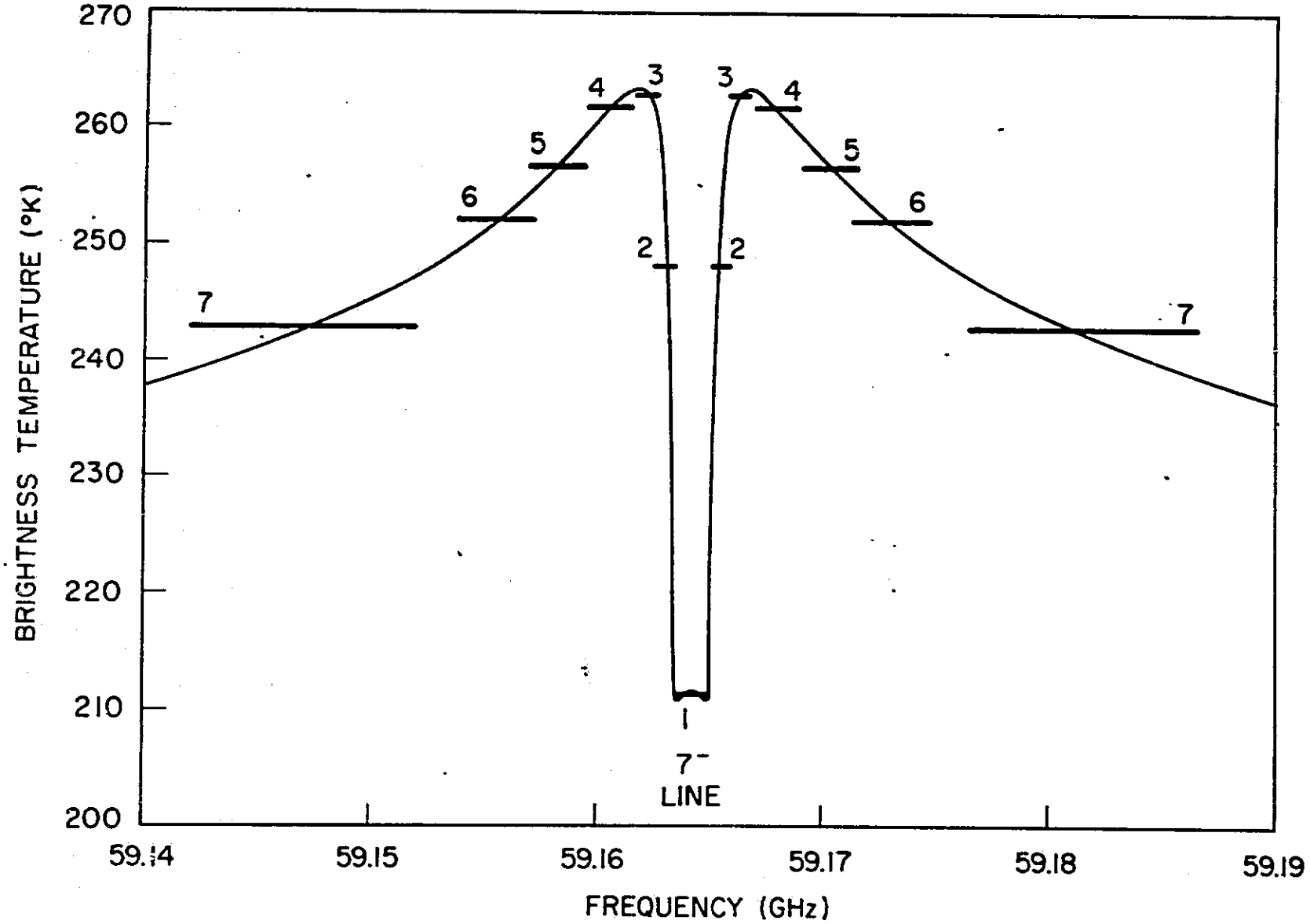

4.1(b) The 7^- line on an expanded frequency scale. The two linear polarizations have been averaged.

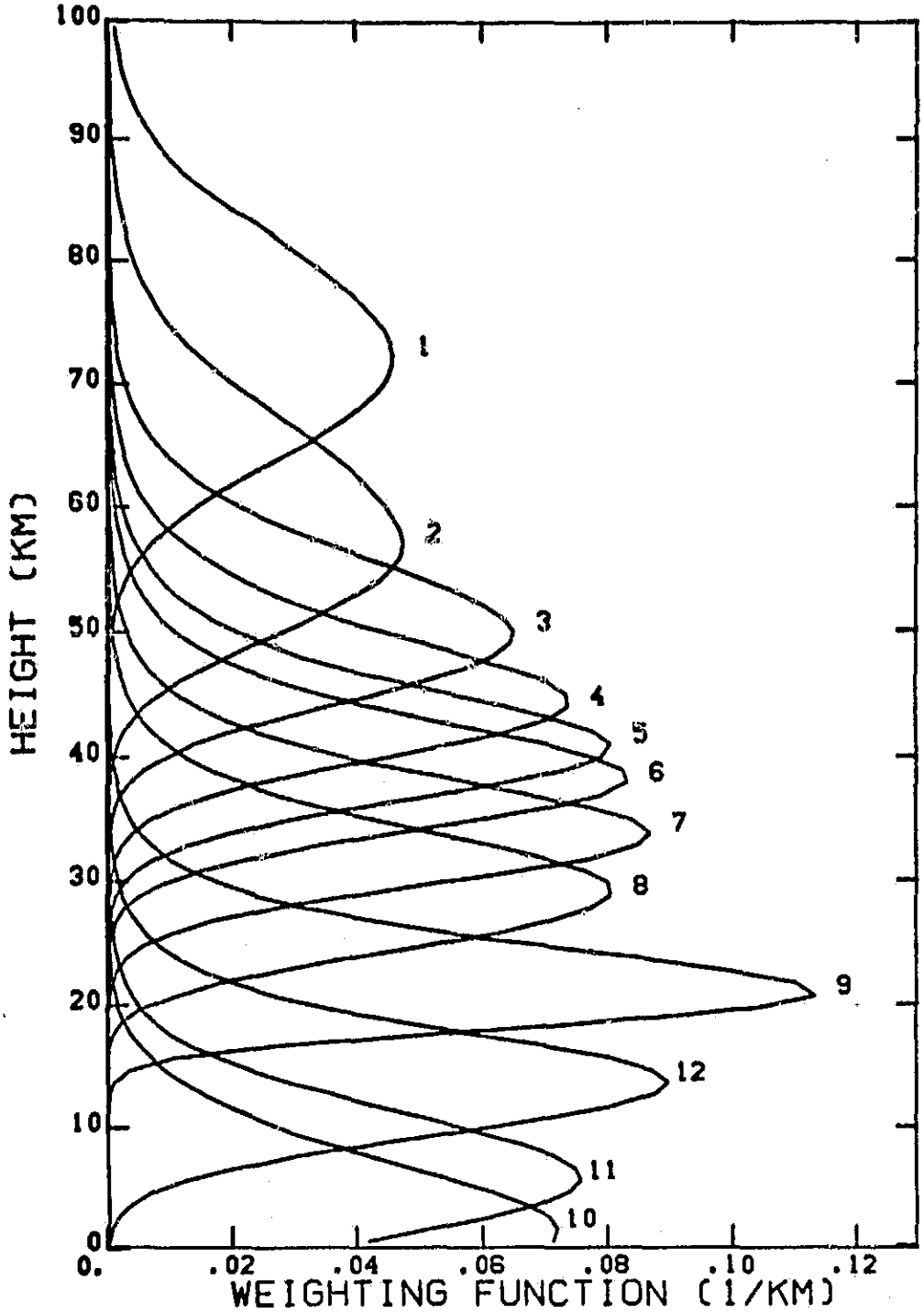

4.2(a) Nadir weighting functions, magnetic equator, linear 11 polarization.

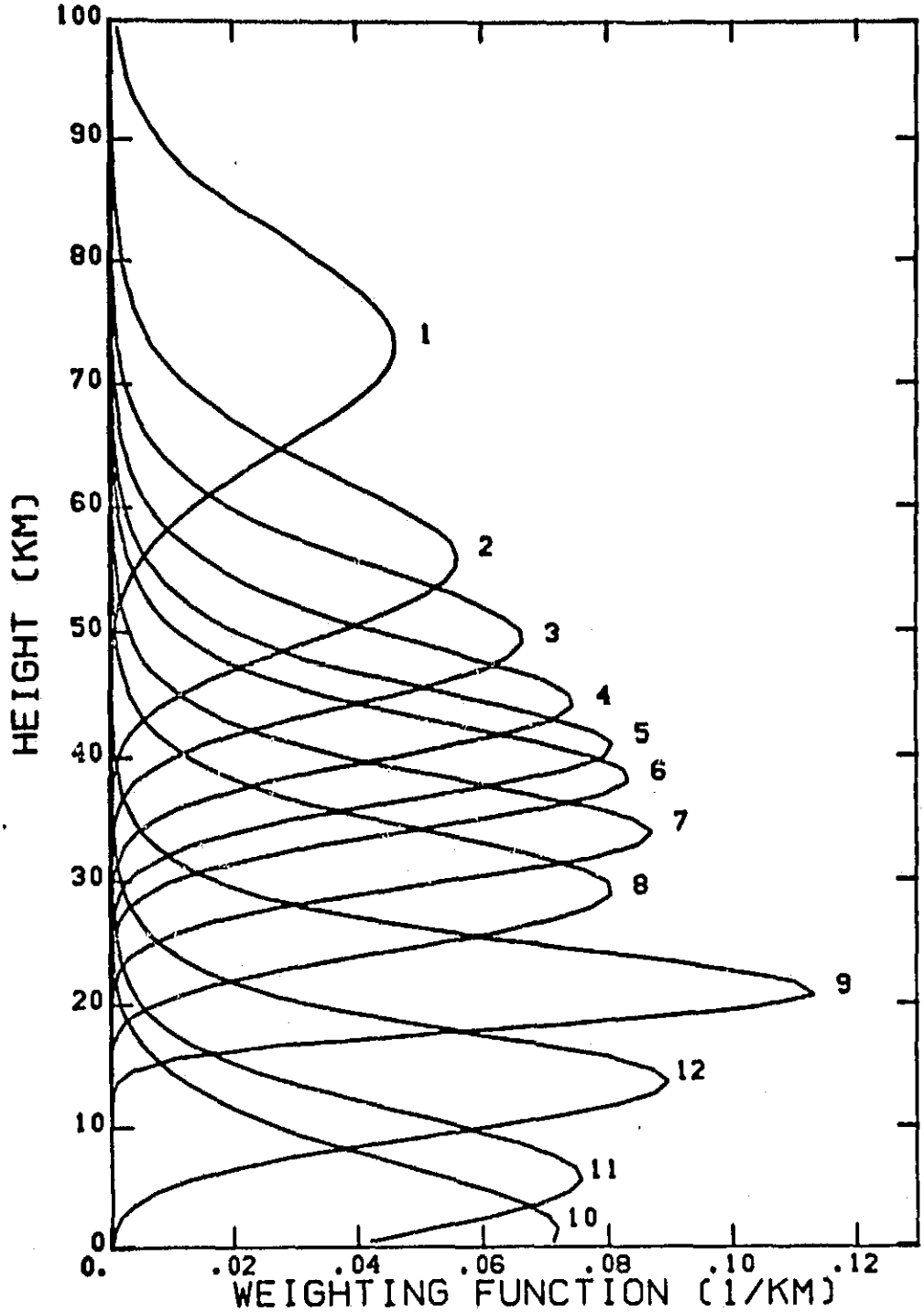

4.2(b) Nadir weighting functions, magnetic equator, linear 22 polarization.

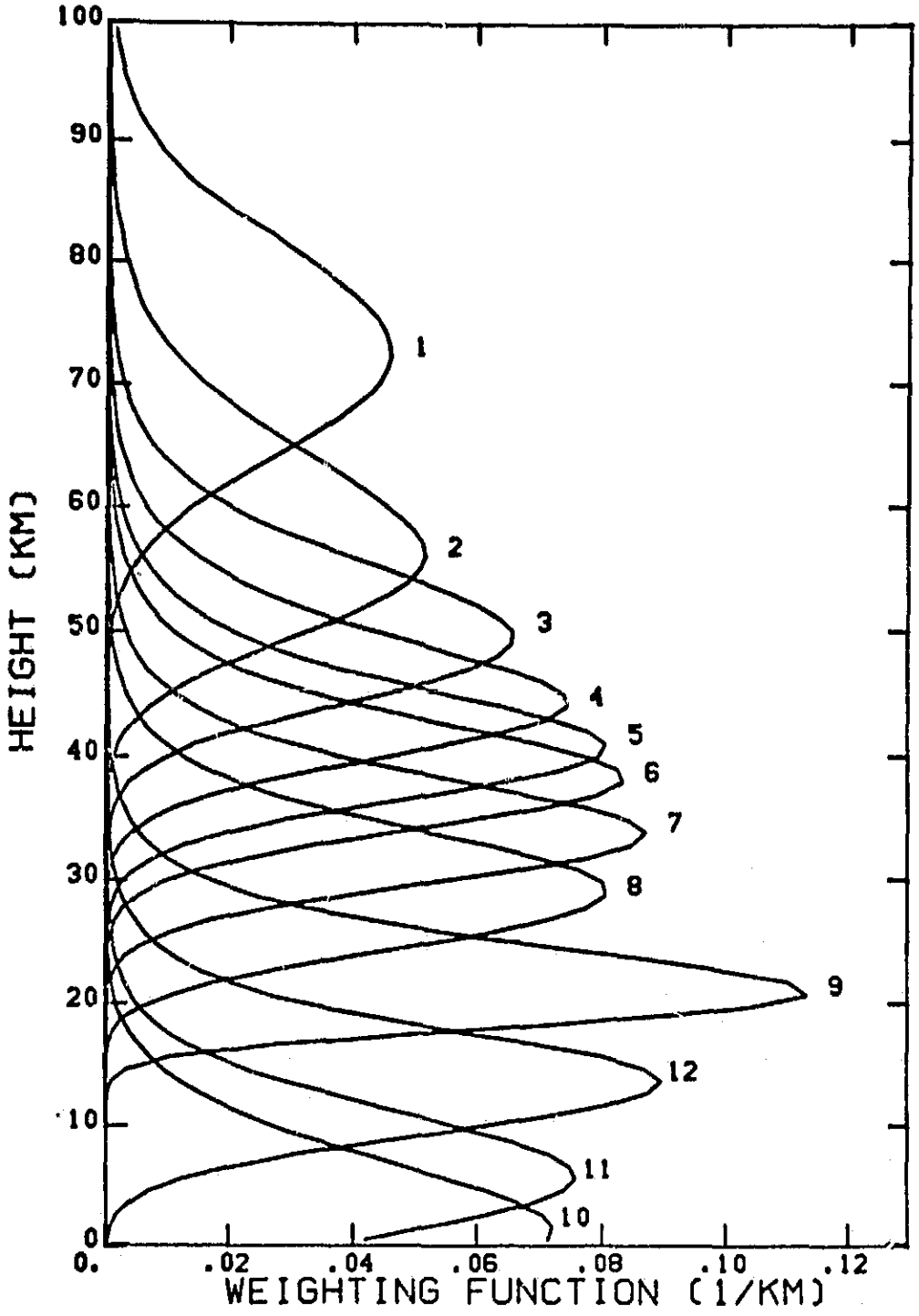

4.2(c) Nadir weighting functions, magnetic equator, circular polarization.

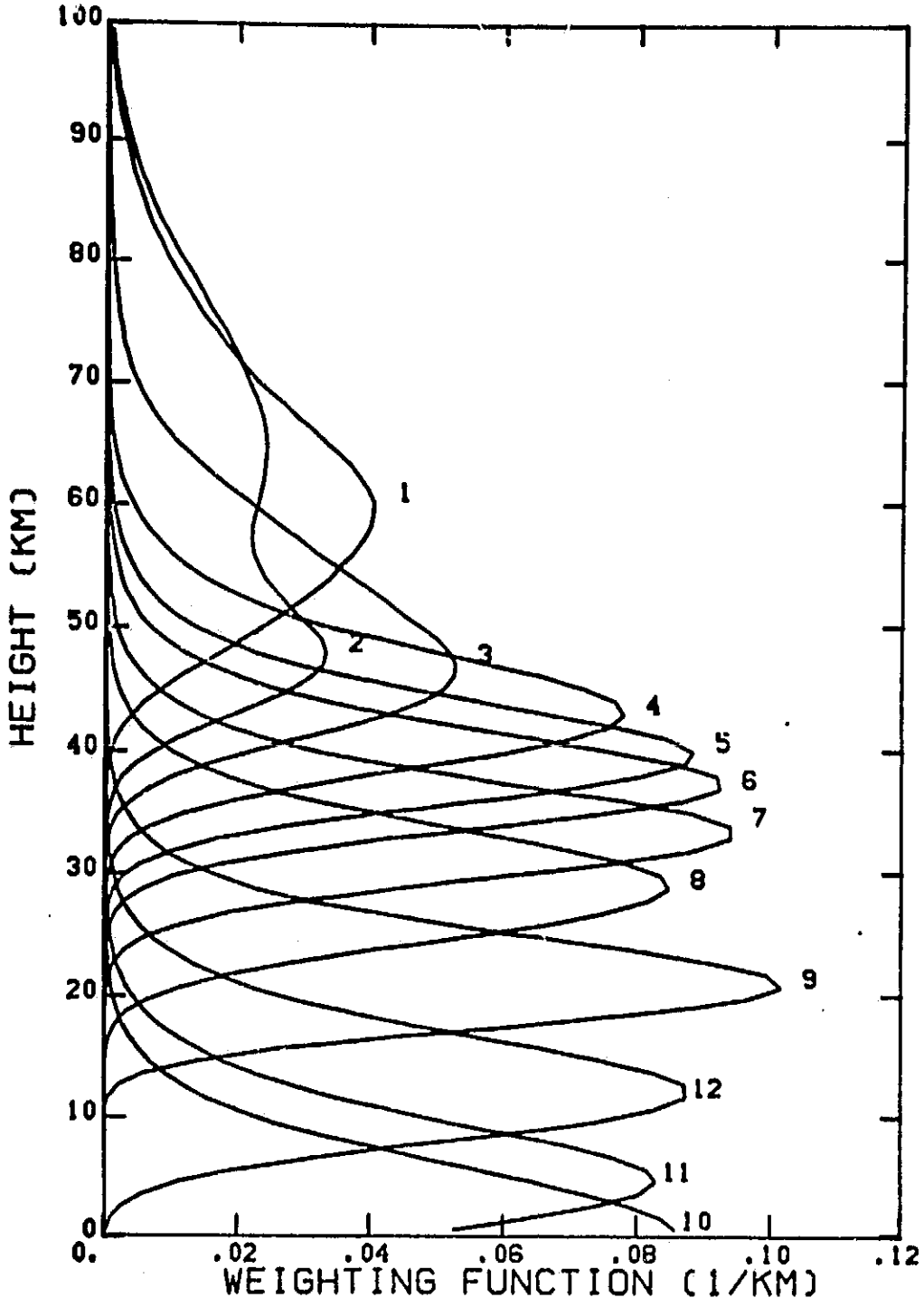

4.2(d) Nadir weighting functions, magnetic pole, circular polarization.

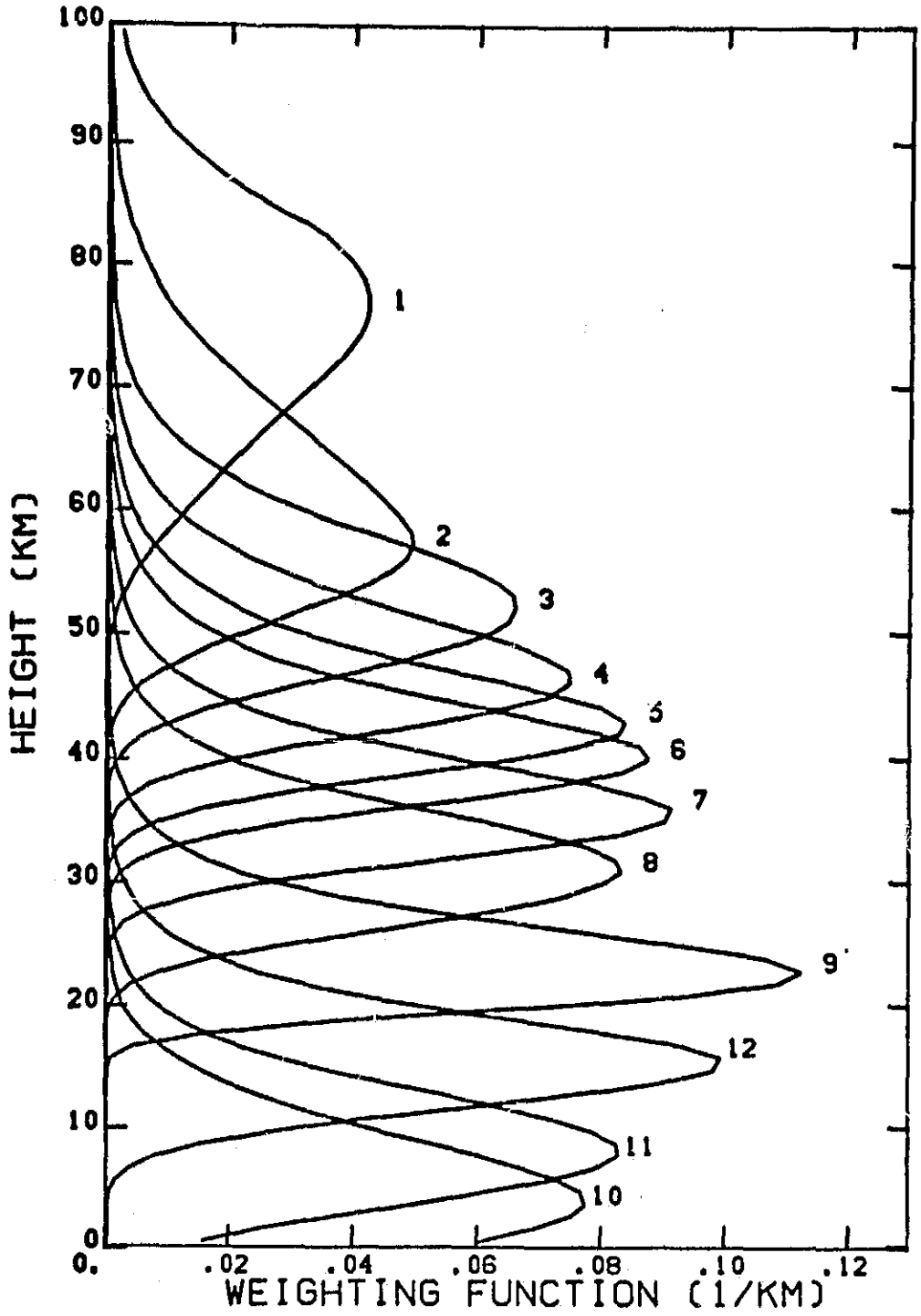

4.2(e) 53.5° weighting functions, magnetic equator, circular polarization, looking north.

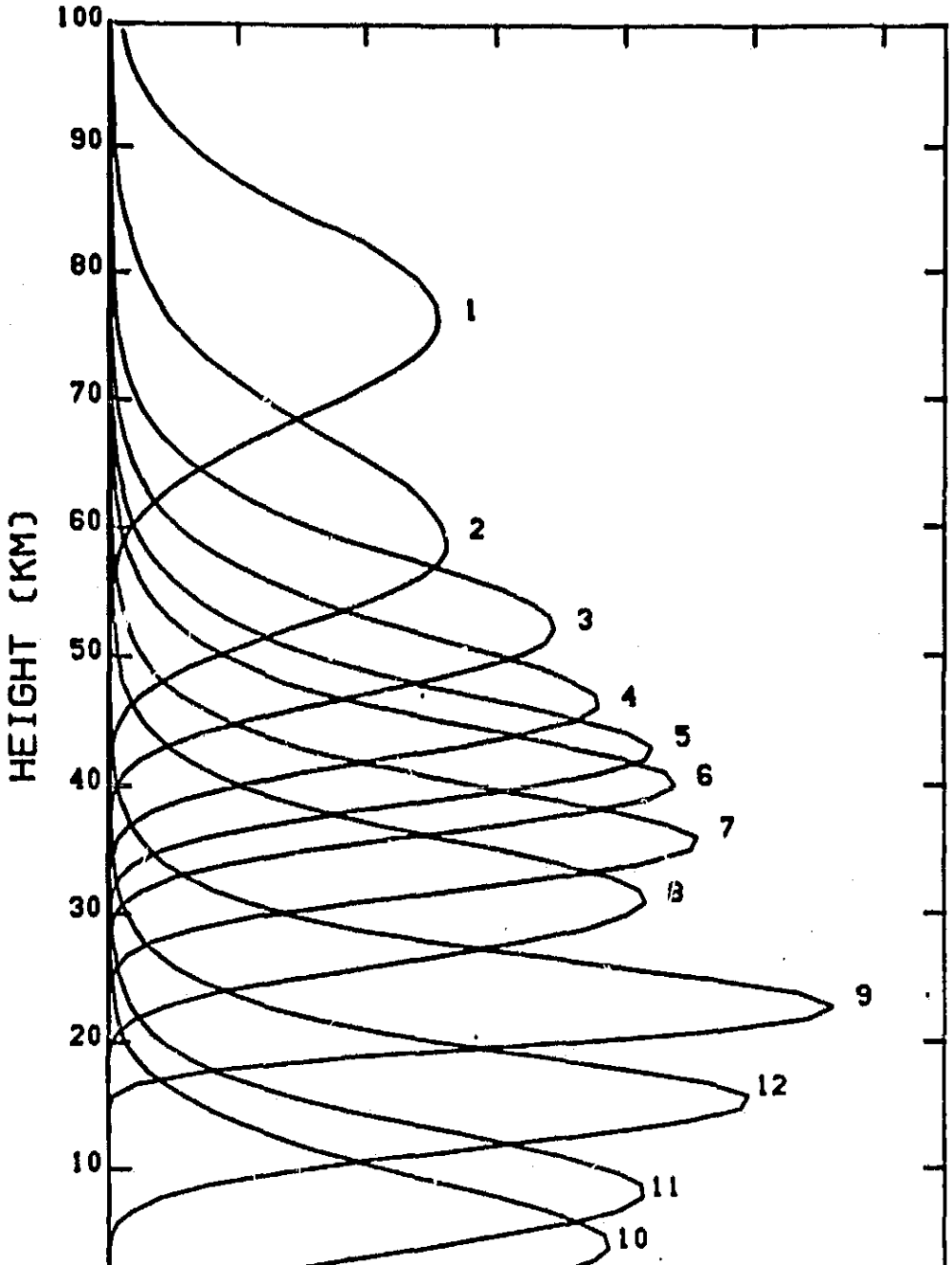

4.2(f) 53.5° weighting functions, magnetic equator, circular polarization, looking east.

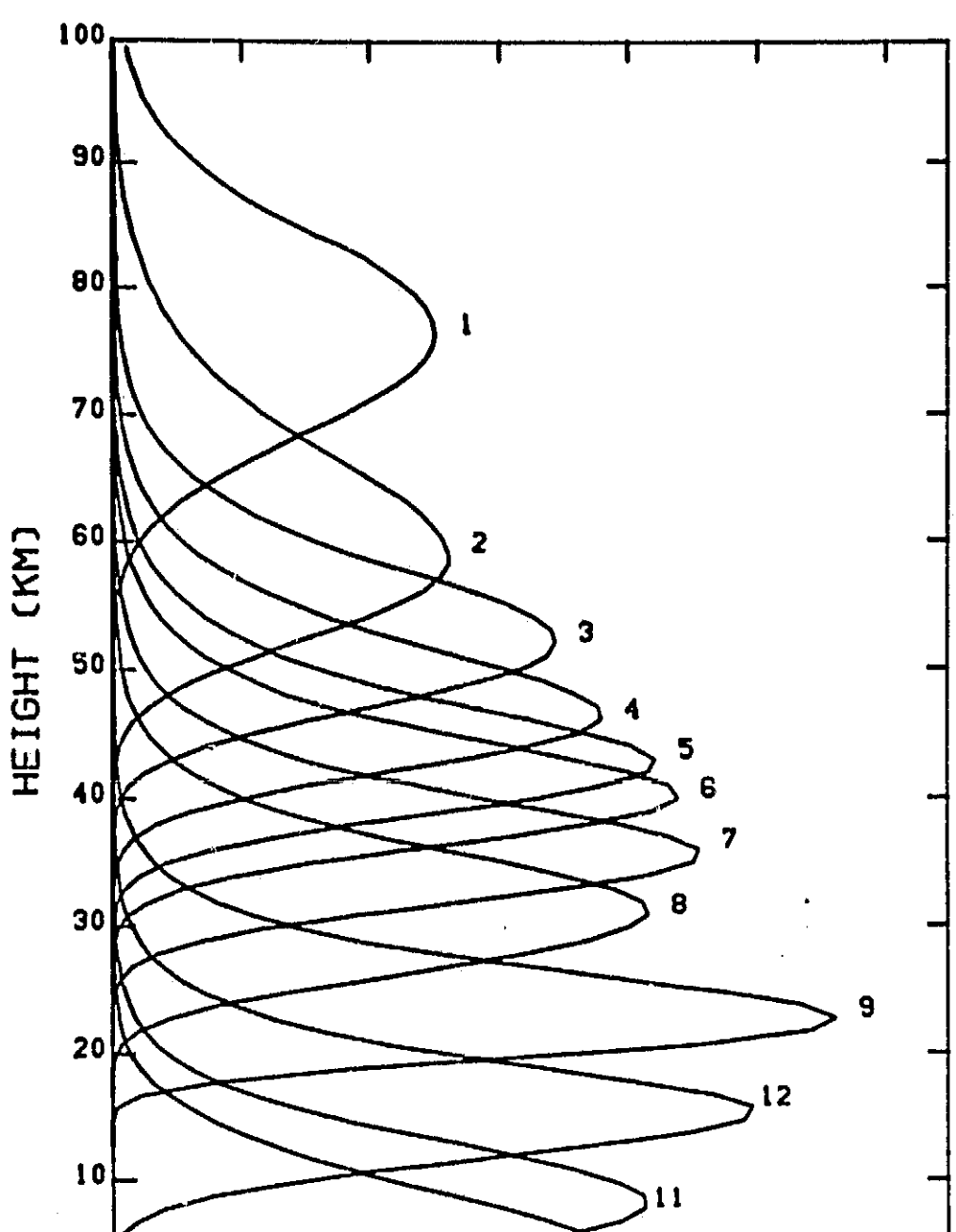

4.2(g) Same as (f) but with lines Doppler shifted.

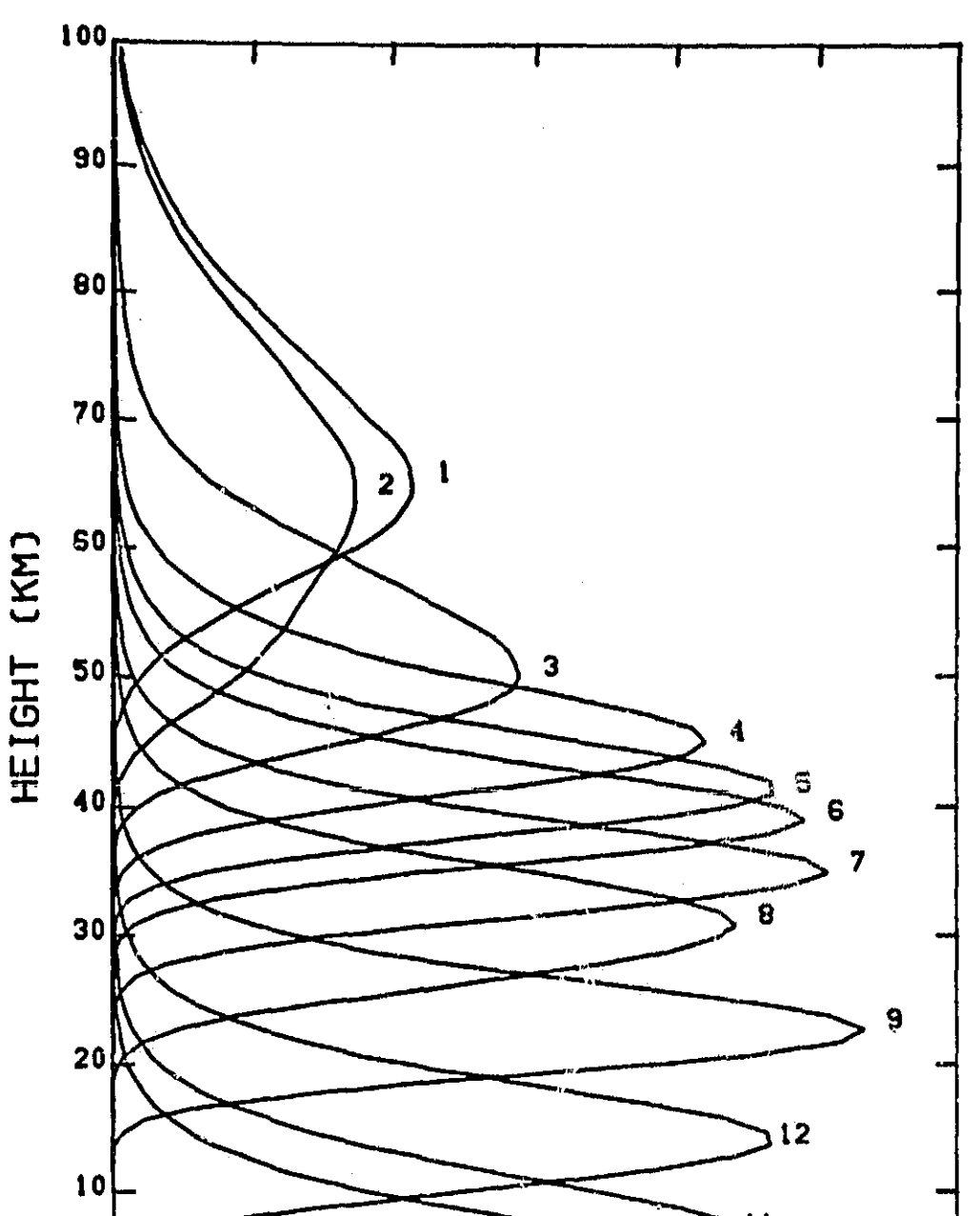

4.2(h) 53.5° weighting functions, magnetic pole, circular polarization.

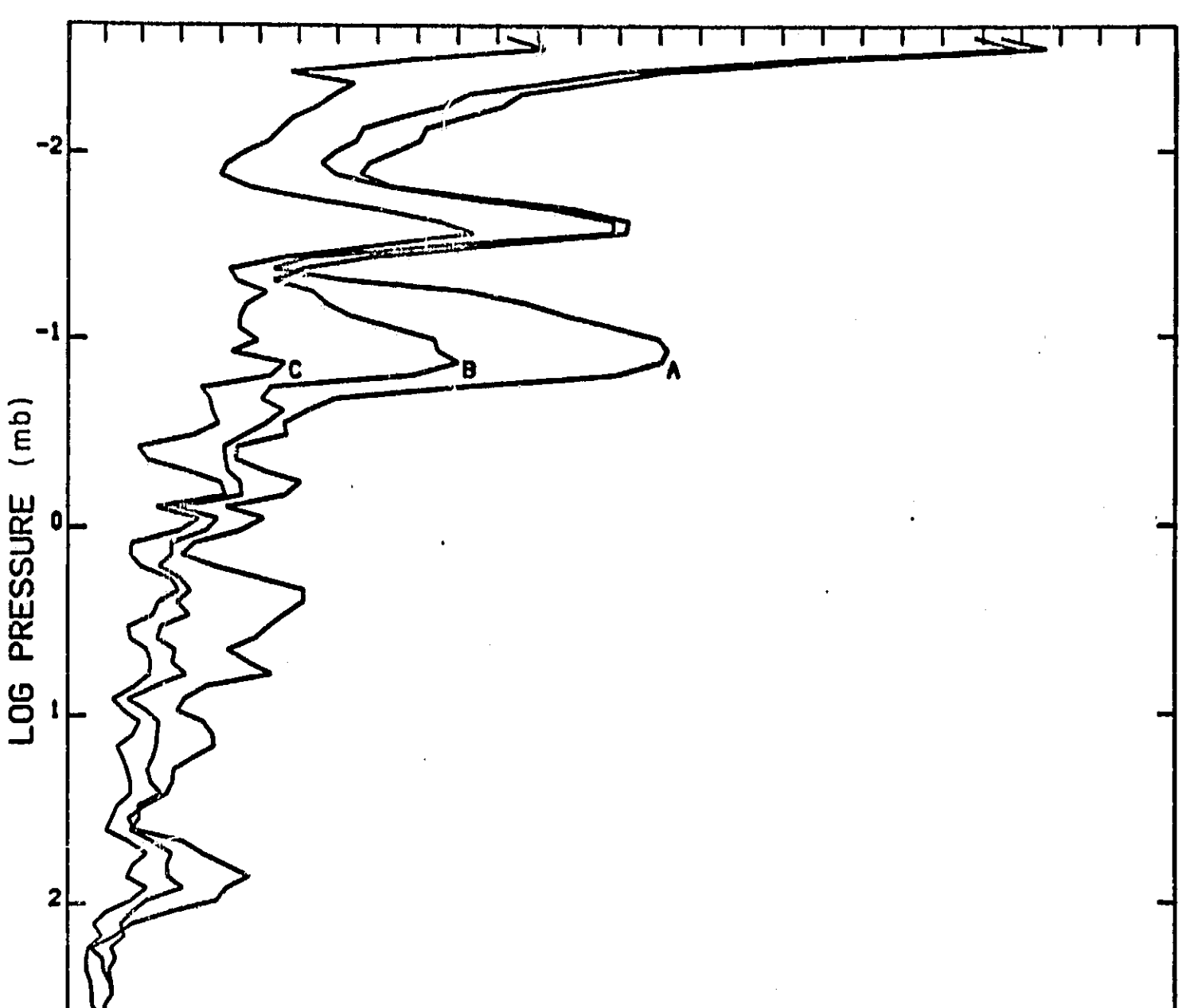

4.3 RMS residuals. The vertical scale corresponds to 0-90 km in height. A - a priori. B - minimum information. C - statistical inversion.

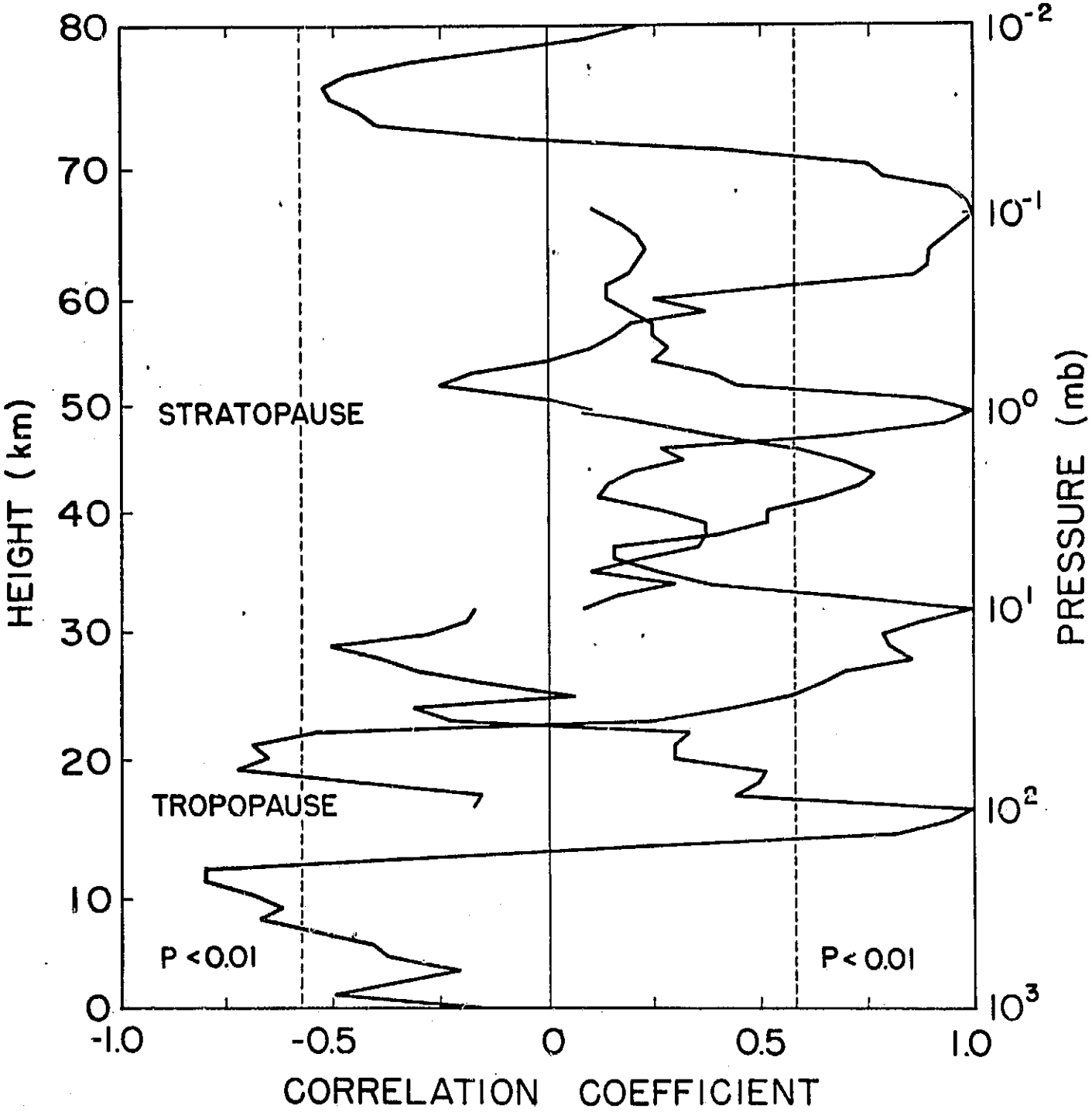

4.4 Correlation coefficients for atmospheric temperatures. Dashed lines show the 1 % probability significance levels.